ALMA MATER STUDIORUM
UNIVERSITÀ DI BOLOGNA

DOTTORATO DI RICERCA IN

TECNOLOGIE INNOVATIVE E USO SOSTENIBILE DELLE RISORSE DI PESCA E BIOLOGICHE DEL MEDITERRANEO (FISHMED-PHD)

Ciclo 38

Settore Concorsuale: 03/D1 - CHIMICA E TECNOLOGIE FARMACEUTICHE, TOSSICOLOGICHE E NUTRACEUTICO - ALIMENTARI

Settore Scientifico Disciplinare: CHIM/11 - CHIMICA E BIOTECNOLOGIA DELLE FERMENTAZIONI

DEVELOPMENT OF MICROBIOME-BASED BIOPROCESSES FOR SUSTAINABLE PRODUCTION OF BIO-RESOURCES FOR THE TEXTILE INDUSTRY

Presentata da: Andrea Nicolò Dell'Acqua

Coordinatore Dottorato

Mauro Marini

Supervisore

Marco Candela

Co-supervisore

Elena Biagi

Esame finale anno 2026

Summary

INTRODUCTION

Ecological role of secondary metabolites

Microbial secondary metabolites are a diverse ensemble of bioactive small molecules produced by microorganisms; they derive their name in opposition to primary metabolism, which is devoted to energy production and cellular growth. While secondary metabolism lack a role in the internal economy of the producing organisms

(Williams and Maplestone , Williams, Stone et al. 1989), while not directly contributing to their growth, it plays a significant role in their adaptation and response to the varying environmental conditions found in the wild, ultimately leading to an increased fitness (Firn and Jones 2000, Tyc, Song et al. 2017). For these reasons, many secondary metabolites are produced only under specific conditions, to carry out specialized functions, for example, microorganisms living in close association with corals, where they may contribute to the protection of the host organism through antibiotic and antifouling functions (Modolon, Barno et al. 2020, Qiu, Gu et al. 2024). Or increase the chances of coral larval attachment and metamorphosis, as it is the case of Brominated compounds produced by *Pseudoalteromonas* sp. harboring the *bmp* biosintetic gene cluster, which encodes the antibiotic pentabromopseudilin and related brominated natural products, thus playing a critical role in the life cycle of corals (Modolon, Barno et al. 2020). The production of siderophores and metallophores is also ecologically relevant, these natural products allow microbial growth in environment with limited Iron content, as producing strains can outcompete non-producing organisms, regulating local microbial composition (Sandy and Butler 2009, Tyc, Song et al. 2017). While the rhizosphere microbial community can mediate other ecologically relevant and diverse functions, here microorganisms living in close association with plants produce an array of secondary metabolites with functions such as quorum sensing, antibiotic and plant-cell's growth-stimulation, contributing to the development and health of the host organism (Tyc, Song et al. 2017, Mashabela, Piater et al. 2022, Narayanan and Glick 2022).

Ecological roles of *Alkalihalobacillus*:

The genus *Alkalihalobacillus* comprises Gram-positive, spore-forming bacteria that have been long associated with marine environments (Joshi, Thite et al. 2022) in particular niches characterized by highly salinity levels and oligotrophic conditions (Joshi, Thite et al. 2022). Beside these characteristic adaptations of *Alkalihalobacillus* strains, other phenotypes have been associated to the growth and survival strategies of this group of organisms, such as tolerance to alkaline environment characterized by high pH values, metals tolerance and finaly host association with macroorganisms such as sponges, sea urchins and algae (Rajasabapathy, Ghadi et al. 2020).

As such multiple strains of marine *Alkalihalobacillus* bacteria have been recovered from diverse niches, for example: *Alkalihalobacillus hwajinpoensis* was isolated from East Sea seawater (Yoon, Kim et al. 2004), while *Alkalihalobacillus oceani* (Gupta, Patel et al. 2020) has been isolated from the Indian Ocean seawater (Song, Liu et al. 2016). Beside free-living strains, some exponents of the genus have been isolated in association with other macroorganisms such as *Alkalihalobacillus. algicola* which was isolated during degradation of the brown alga *Fucus evanescens* (Ivanova, Alexeeva et al. 2004). It

showed the ability to grow up to ~3% NaCl while degrading algal polysaccharides (Ivanova, Alexeeva et al. 2004). Another strain, in this case isolated from sponge tissue, *Alkalihalobacillus plakortidis* is alkaliphilic and salt-tolerant, growing at pH 7–11 and in media with up to 12% NaCl (Borchert, Nielsen et al. 2007). Lastly, a novel *Alkalihalobacillus* strain was isolated from the gut of cultured sea urchins (Masasa, Kushmaro et al. 2022).

This adaptability is also recognized by genomic studies carried out on marine *Bacillus*, where genes coding for multiple types of transporters, such as sugar ABC transporters are for carbohydrate degrading enzymes like glycosidases, chitinases and beta-xylosidases are commonly found. Comparative genomics also highlighted how in some strains, metabolism has been streamlined to minimize energy expenditure, while degrading organic matter (Gupta, Patel et al. 2020), hinting at the ability to efficiently metabolize complex carbohydrates giving *Alkalihalobacillus* a better chance of survival, especially in nutrient poor environments or environments characterized by harsh salinity conditions, as well as their possible role as key agents in nutrient turnover in marine environments (Gupta, Patel et al. 2020).

Along-side genes involved in metabolic adaptation to oligotrophic environments, genes for the specialized transport of potassium and sodium ion are present to allow for the maintenance of pH and Ionic homeostasis, along with genes devoted to the accumulation of glycine betaine osmolyte as an adaptative strategy to the presence of high salt concentrations.

Another extensively studied ecological feature of marine *Bacillus*, is their production of secondary metabolites. Biosynthetic gene clusters for the production of compounds such as macrolactins, terpenoids or polyketides can be found inside the genomes of marine *Bacillus* species including *Alkalihalobacillus*. In the environments these compounds act as broad range antimicrobial, enabling the producer influence the composition of microbial communities in the water column, sediments and the host-associated microbiome of algae and sponges (Gupta, Patel et al. 2020, Rajasabapathy, Ghadi et al. 2020).

In the context of host associated lifestyle, *Alkalihalobacillus* strains have often been isolated from marine algae and sponges, in this case *Alkalihalobacillus* strains may participate in mutualistic relationship with the host microorganism, thereby producing protective antimicrobial compounds or by degrading organic matter such as complex polysaccharides with the versatile enzyme suite they possess, which can integrate the diet of sponges or sea urchins (Radovanović, Milutinović et al. 2018), in the case of algal host associations, Alkahalilobacillus strains have been shown to degrade algal tissue and debris produced by the natural growth cycle of algal hosts, as well as to forming a biofilm layer on the algal surface and regulating its microbial compositions (Gupta, Patel et al. 2020). To note is also the ability of some strains to efficiently tolerate and detoxify heavy

metals such as chromium and manganese, through the use of specialized reductase enzymes (Ivanova, Alexeeva et al. 2004), this capability is enhanced when actively growing in a biofilm.

Ecological roles of *Paracoccus*:

The bacterial genus *Paracoccus* is composed by microorganisms with an exceptional ecological and metabolic versatility, this is observable by their world-wide distribution across the globe (Hollensteiner, Schneider et al. 2023). Strains have been isolated from both land and marine environments, such as the case for *Paracoccus* amoyensis wich was isolated from Xianmen coastal waters, as well as in association with living hosts, most often marine animals, these associations could be mutualistic as in the case of *Paracoccus spongiarum* with the sponge phakellia elegans, or in the case of *Paracoccus nototheniae* with antartic fish *nototheniae coriiceps* (Kämpfer, Irgang et al. 2019, Lyu, Lai et al. 2021, Kim, Kim et al. 2024). The switch to an opportunistic behavior has been hypothesized, as a *Paracoccus* strain was isolated from crabs heavily affected by black spot disease, as well as from comparative genomics investigations where some of the mechanisms employed by *Paracoccus* strains during commensal or mutualistic host-associations could be repourposed for opportunistic interactions (Carlos, Pereira et al. 2017, Zhang, Zeng et al. 2023).

In line with their global presence, we see that *Paracoccus* strains are capable of performing a variety of key environmental functions, for example multiple strains of *Paracoccus* such as, *P. aerodenitrificans*, *P. sediminicola* and *P. albus*, isolated from river sediments, have shown the capability to perform Heterotrophic nitrification–aerobic denitrification (HN-AD), a versatile pathway with which nitrification and denitrification processes can occur within the same cell, greatly facilitating the removal of fixed nitrogen from the environment, which is transformed and released as inorganic gaseous N2 (Jaffer, Sanath Kumar et al. 2019, Leinberger, Holste et al. 2021).This characteristic allows *Paracoccus* strains to close the marine nitrogen cycle, particularly important in coastal shrimp ponds or eutrophic waters where the balance of nitrogen can be critical for the health of aquatic organisms.

Following through, a number of *Paracoccus* strains have shown the ability oxidise highly reduced and toxic sulphur compounds through the use of Sox enzyme system (Jaffer, Sanath Kumar et al. 2019), which not only allows for the final production and release of sulphate ion (SO_4^{2-}), a critical component in the biogeochemical cycle of sulphur and the main form of sulphur absorbed by plants and by some bacteria. The process also yields the production of ATP inside of *Paracoccus* cells, making them facultative lithoautotrophic bacteria, further increasing the possible niches inhabitable by exponents of this genus (Kumdhitiahutsawakul, Jirachaisakdeacha et al. 2022).

To complete the picture, *Paracoccus* species can contribute to phosphorus cycling with a number of strains reported to assimilate phosphate rapidly while growing under oligotrophic conditions (Mei, Wu et al. 2019, Varasteh, Hamerski et al. 2021, Deng, Li et al. 2024). To thrive under low nutrient conditions or in environments where nutrient levels can fluctuate greatly in quantity and composition, such as ice microenvironments in polar regions or when living in association with corals in oligotrophic waters, *Paracoccus* strains have been selected to possess a repertoire of enzymes capable of metabolizing a vast variety of carbon substrates including complex carbohydrates, polyols, amino sugars, and various low-molecular-weight organic acids. Adding on, several strains possess pathways for polyhydroxyalkanoate (PHA) synthesis and accumulation, which allow them to store excess carbon when growth is limited by nitrogen or oxygen, leading to the formation of PHA granules inside the cell (Carlos, Pereira et al. 2017).

From metagenomic studies it has been revealed that exponents of the *Paracoccus* genus possess genomes enriched in mobile genetic elements of different types, including insertion sequences, transposase sequences, genomic islands and prophages. In particular these elements have been linked to horizontal gene transfer events. This particular evolutive strategy appears to be a defining characteristic of the *Paracoccus* genus, as the open pangenome of *Paracoccus* indicates that these bacteria continually acquire novel genes, that allow for the adaptation to new environments by expanding their core genome with genes involved in sugar metabolism, nutrient acquisition, stress tolerance, and host interaction relevant for specific niches (Carlos, Pereira et al. 2017, Hollensteiner, Schneider et al. 2023). Along with mobile genetic elements, strains have been shown to possess gene clusters encoding type II and type IV secretion systems, enabling the exchange of genetic information, as well as effector molecules, involved in nutrient acquisition, stress tolerance, and host interaction. It has been speculated to make them hub for the exchange of adaptive traits within marine microbial communities.

Besides having a recognized role in the biogeochemical cycles of nutrients, *Paracoccus* strains have been shown to harbour BGCs for the production of functional molecules such as: siderophore, exopolisaccarides, bacteriocins, non-ribosomal peptides, carotenoids and poliketides(Leinberger, Holste et al. 2021). Along with the propensity of *Paracoccus* strains to transfer and obtain advantageous genomic mobile elements, the genomes of strains inhabiting different niches may undergo a pronounced loss of genes in order to streamline their overall metabolism retaining the most important functions related to each niche.

For example free-living strains usually harbor larger genomes, with a greater abundance of mobile elements compared to their host-associated counterparts, to account for the different selective pressures than may be encountered in the open marine

environments, and also generally present an enrichment in genes for type IV secretion systems and genes that promote genetic exchange within biofilms, wich could be intended as a momentary exit strategy from the free living lifestye, when marine conditions turn higly unfavourable. Eventually this process could lead to colonization of a new niche, with the development of niche specific adaptations, for example strains living in host-associated environments, possess an enhanced production of pigments, such as carotenoids, that contribute to the antioxidant capacity of *Paracoccus* cells which may extend to protect host tissues from oxidative damage, under conditions of high light and reactive oxygen species (Leinberger, Holste et al. 2021), the synthesis of carotenoid pigments by *Paracoccus* strains associated to corals, might also have implications in the correct metamorphosis of the host, throughout its life cycle (Varasteh, Hamerski et al. 2021).

In the context of interactions with corals hosts, certain *Paracoccus* strains are able to produce exopolysaccharides. Succinoglycan is particularly noteworthy, as its production has been linked to the capacity of *Paracoccus* strains to aggregate and attach to coral surfaces in high-osmolarity, oligotrophic conditions, but most importantly to a stabilizing effect over the growth of biofilm, thereby controlling microbial consortia on host tissues preventing extensive biofilm overgrowth that might trigger pathogenic outcomes (Carlos, Pereira et al. 2017). In addition, these exopolysaccharides may also facilitate interactions with other marine invertebrate hosts, like bryozoans and crustaceans, from which *Paracoccus* species have been isolated where they are implicated in both mutualistic and opportunistic behaviours. Lastly, in these niches, *Paracoccus* bacteria often exhibit streamlined genomes which privilege: specialized transporters for substrate exchange, enhanced capacity for adhesion, and stress-protective enzymes that facilitate survival in host environments (Leinberger, Holste et al. 2021, Varasteh, Hamerski et al. 2021).

Lastly, one final activity of selected *Paracoccus* strains, which is removed from the previously described functions involved in biogeochemical cycles and host associations, is their potential algicidal activity and control of blooming algae populations.

Paracoccus Strain Y42, has presented a potent algicidal activity against dinoflagellates like *Prorocentrum donghaiense*, that is notorious for causing harmful algal blooms (HABs). The algicidal substances secreted by this strain, seem to remain stable over a wide range of environmental conditions, across diverse temperatures and pH levels (Varasteh, Hamerski et al. 2021). They were found to damage the thylakoid membranes and compromising photosystem II efficiency, which can lead to oxidative stress and lipid peroxidation in the algal cells (Zhang, Ye et al. 2018).

This activity not only modulates algal biomass but also contributes to the overall regulation of phytoplankton communities and offers a potential starting point for the

development of ecofriendly strategies for the management of blooming events (Zhang, Ye et al. 2018).

Ecological roles of *Cladosporium*:

The fungal genus *Cladosporium* is comprised of a group of cosmopolitan ascomycetes(Salvatore, Andolfi et al. 2021). These fungi have been found to be ecologically versatile, inhabiting diverse marine environments where they significantly contribute to nutrient recycling (Cunliffe, Hollingsworth et al. 2017),in this context *Cladosporium* fungi have been found to participate in saprotrophic decomposition of complex organic substrates such as algal detritus, seagrass litter, lignocellulosic wood, and hydrocarbons while also engaging as endophytes, opportunistic pathogens, or epiphytes on marine hosts (Cunliffe, Hollingsworth et al. 2017). Originally hailing from terrestrial niches, many *Cladosporium* species appear to have transitioned back to marine environments, this endowed them with remarkable adaptations such as halotolerance, psychrotolerance, along with the production of extracellular enzymes tolerant to low temperatures and high salt concentrations such as glucan 1,3-β-glucosidase, cellulases, lignin peroxidases, laccases, and endoxylanases (Muriel, Bruque et al. 1996, Salvatore, Andolfi et al. 2021).

Cladosporium species constitute key saprobes and are responsible for degrading a wide variety of recalcitrant organic materials accumulating in marine ecosystems, such as diatom-derived polysaccharides, lignocellulosic debris and other complex carbohydrates, facilitating the release of organic carbon and essential nutrients in nutrient-poor marine environments (Cunliffe, Hollingsworth et al. 2017, Salvatore, Andolfi et al. 2021). Their activity is also dependent on habitat composition, in regions such as oil-polluted sediments Cladosporium species contribute to the biodegradation of aliphatic hydrocarbons (Salvatore, Andolfi et al. 2021) while in coastal habitats, these fungi decompose seagrass detritus or mangrove litter, altering its biochemical composition and carbon-to-nitrogen ratios through the release of amino acids, polyunsaturated fatty acids, and vitamins that become available to a wider range of marine detritivores. Lastly Cladosporium species have been found in deep chlorophyll maxima, a layer of subsurface water where chlorophyll concentration is the highest, there they associate with algal particulate organic matter, degrading algal glucans (Cunliffe, Hollingsworth et al. 2017, Chrismas and Cunliffe 2020).

Additionally, Cladosporium species have been found to interact with marine macroorganisms in a variety of complex ways; Cladosporium cladosporioides has been implicated in pathogenic interactions with the marine alga Pseudendoclonium submarinum under controlled culturing conditions, where the fungus invades interstitial spaces between algal filaments, leading to chlorophyll loss and cell necrosis (Cunliffe,

Hollingsworth et al. 2017), however, in situ observations often reveal a more benign, asymptomatic colonization, suggesting an “endophytic continuum” where host stress, senescence, or environmental shifts may trigger a transition to a pathogenic state. In natural environments Cladosporium strains often maintain epiphytic lifestyles on surfaces of macroalgae and seagrasses, becoming integral part of algal biofilm, without inducing overt host damage, these associations may confer adaptive advantages for both host and fungus, potentially enhancing host defence against other pathogens through the production of antifouling or antimicrobial secondary metabolites.

Cladosporium strains are also frequently encountered in association with marine sponges, seagrasses, and corals. In sponges, for example, Cladosporium has been isolated as both a resident and transient member of the mycobiome, contributing to nutrient cycling within the sponge holobiont and potentially offering protective benefits through the secretion of bioactive compounds (Salvatore, Andolfi et al. 2021). Similarly, endophytic colonization of seagrass tissues by Cladosporium may promote host growth and increase resistance to environmental stressors, while also participating in the degradation of senescent tissues and recycling of nutrients back into the ecosystem (Salvatore, Andolfi et al. 2021).

To effectively colonize a wide variety of niches marine Cladosporium fungi are characterized by a robust enzymatic machinery, secreting a diverse spectrum of extracellular enzymes. Key among these is the secretion of glucan 1,3-β-glucosidase, which facilitates the digestion of phytoplankton-derived organic matter and contributes to efficient carbon assimilation (Muriel, Bruque et al. 1996). In addition to polysaccharide-degrading enzymes, numerous marine Cladosporium species produce ligninolytic enzymes like laccase, manganese peroxidase, and lignin peroxidase, which catalyse the breakdown of lignin and aromatic compounds from mangroves and seagrasses (Muriel, Bruque et al. 1996).

Secondary metabolites production also supports Cladosporium strains in colonizing different niches, various classes of natural products have been produced by Cladosporium, poliketides, alkaloids, steroids and terpenoids which have been shown to possess antimicrobial, antiviral and antinflamatory properties to confer resistance against environmental stressors alongside shaping the structure and dynamics of local microbial communities (Salvatore, Andolfi et al. 2021).

Pigments in the past

Colours have always been a fundamental component of our daily lives, present everywhere—from the natural world around us to the objects and clothing we use. They

not only define aesthetics, but often deeply influence our perception and emotional state (Yildirim, Akalin-Baskaya et al. 2007). The fascination that colours exert on human beings prompted an early search for usable pigments: the first ones, used since the Upper Paleolithic in cave paintings, were mineral-based, such as ochres—yellow and red colours obtained from minerals like limonite and hematite (Velliky, Porr et al. 2018).

The earliest dyes appear to date back to the ancient Egyptians (Abel 2012); these were of natural origin, usually plant-based, like the purple-red extracted from lichens of the Roccella genus, yellow from saffron, and blue from indigo (*Indigofera tinctoria*) and woad (*Isatis tinctoria*) (Abel 2012). Over time, colours became a symbol of social status; in Greco-Roman times, laws prohibited anyone except kings and aristocrats from wearing purple—a highly coveted colour due to the difficulty of obtaining it from *Murex* sea-snails, which had to be crushed or pricked to stimulate secretion. It took about 12,000 snails to yield just 1.4 grams of pure dye (Abel 2012).

Later, in the Middle Ages, the development of painting and the arts in general became the main impetus for discovering new colours and improving dyeing processes to obtain more stable hues. Until that time, producing vivid and lasting dyes was complex, costly, and required large amounts of raw materials—often hard to source or work with—thereby restricting the use of pigments to certain social classes.

Development of synthetic dyes

A radical change occurred in 1856 with the synthesis of the first artificial textile dye, Mauveine, which was accidentally discovered by William Henry Perkin while attempting to synthesize quinine for antimalarial use (Cova, Pais et al. 2017). Although Mauveine remained on the market for only a few years, it marked a groundbreaking turning point that made the wide range of colours we now take for granted accessible to everyone. The synthetic dye industry triggered a revolution in industrial and textile chemistry, leading to the ever-growing production of synthetic pigments, eventually reaching today's volume of around one million tons per year (Tkaczyk, Mitrowska et al. 2020).

However, over time, the globalization of the textile system and large-scale pigment production at low cost have come with a significant environmental toll, causing serious negative effects on ecosystems and lasting consequences on natural balance.

Difference between dyes and pigments

The difference between dyes and pigments is independent of their origin and instead concerns their chemical nature. Dyes are very small molecules, soluble in water and other solvents, capable of penetrating the material and colouring it in a permanent and

uniform way. Pigments, on the other hand, are larger particles—up to 500 times the size of dye molecules—and are insoluble in water and other solvents. As a result, they settle on the surface of the material as crystals, without being absorbed.

In biological literature, as well as in this context, the terms dye and pigment are not always used strictly according to their chemical definitions (Fried, Oprea et al. 2022). In the following sections, whether referring to a pigment or a dye, the term will generally indicate coloured molecules of natural origin—that is, a coloured biological metabolite—or of synthetic origin.

Chemical classification of natural pigments

Pigments can be classified in various ways—according to their solubility, their natural or synthetic origin, their organic or inorganic nature, or even their hue (Shen, Ren et al. 2023). In this context, we will briefly explore a classification of pigments based on their basic chemical structure, as it best highlights their distinctive characteristics (Shen, Ren et al. 2023).

Polyphenols

Polyphenolic pigments, abundantly found in nature, are characterized by structures that include one or more aromatic rings with hydroxyl groups (Shen, Ren et al. 2023). Among the most widespread and significant polyphenols are flavonoids, common plant secondary metabolites, often bound to glucosides or in free form, which have the ability to protect the plant from excessive radiation and neutralize free radicals. Therefore, they play an antioxidant role in addition to their typical signalling function of providing bright colours to attract pollinating insects.

Flavonoids generally exhibit hues ranging from pale yellow to bright orange, but some subgroups—such as anthocyanins—produce distinctive colours like purple, visible in fruits and vegetables such as apples, blackberries, grapes, blueberries, and eggplants (Shen, Ren et al. 2023). Although most polyphenols are insoluble in water, anthocyanins are highly soluble and show marked sensitivity to factors like pH, light, and temperature, which affect their colouration. This makes them useful as pH indicators in food packaging for monitoring food freshness.

Polyphenolic pigments in general are widely used in the food industry as alternatives to synthetic dyes, providing vibrant colour to beverages and sweets (Shen, Ren et al. 2023). A well-known polyphenolic pigment is curcumin, a yellow substance extracted from turmeric rhizome. In the past, it was used as a textile dye, but due to weak interactions with fibres, the colour tended to fade with washing, limiting its use in fabrics (Zhou and Tang 2016).

Carotenoids

Carotenoids are naturally occurring lipophilic pigments, with colours ranging from yellow to red, abundantly found in plants and photoautotrophic organisms. They represent the second most common class of pigments in nature, after melanin (Shen, Ren et al. 2023). To date, over 800 types have been identified, found in fruits, vegetables, and also produced by bacteria, algae, fungi, and yeasts.

Structurally, carotenoids are tetraterpenoids, characterized by a linear hydrocarbon chain of 40 carbon atoms (C40) that includes a series of conjugated double bonds. This structure forms a system capable of absorbing light and producing the vivid colours typical of carotenoids (Shen, Ren et al. 2023).

Essential for photoautotrophic organisms, carotenoids participate in photosynthesis and play a key role in photosystem assembly and light harvesting, protecting cells from excess radiation and neutralizing free radicals. Around 50 carotenoids can be converted into vitamin A, which is crucial for vision, development, and the immune system in both humans and animals. These provitamin A carotenoids are also known for their antioxidant properties, which is why a diet rich in carotenoids is associated with a lower risk of certain cancers and cardiovascular diseases (Shen, Ren et al. 2023).

Beyond their use as food colourants, carotenoids are also used in cosmetics, for example as ingredients in self-tanners and sunscreens (Shen, Ren et al. 2023). However, they are not employed as textile dyes, as tests have shown that fabrics dyed with carotenoids are poorly lightfast and tend to fade (Baaka, El Ksibi et al. 2017).

Indoles

Indoles are aromatic compounds composed of a benzene ring fused with a pyrrole ring, which display colouring properties due to the presence of conjugated double bonds. Melanin is the most widespread indolic pigment in nature; it is poorly soluble and displays a chromatic range from black to light brown, sometimes with reddish or greenish hues (Shen, Ren et al. 2023). It is known to be produced by melanocytes, contributing to skin pigmentation within humans and other tetrapods. Melanin synthesis is stimulated by exposure to sunlight, activating a protective mechanism against damage caused by UV radiation.

There are different forms of melanin: eumelanin, pheomelanin, and allomelanin, which perform a protective role primarily against light radiation, reactive oxygen species, and chemical stress (Shen, Ren et al. 2023).

Melanin is also produced by bacteria and fungi from dihydroxynaphthalene precursors, serving an adaptive function against environmental stresses (Tran-Ly, Reyes et al. 2020, Singh, Nimse et al. 2021). Melanin is used in cosmetics, for example in sunscreens, where it acts as a UV filter. It is also employed in the food industry to prevent oxidation

and as an antibacterial additive for preservation purposes. Melanin appears to be applicable in textile dyeing as well—some studies have demonstrated its good colouring ability on wool, along with wash fastness and light resistance (Shen, Ren et al. 2023) (Singh, Nimse et al. 2021).

Anthraquinones

Anthraquinones represent a large family of natural pigments, with over 700 compounds identified—most of them originating from lichens, fungi, and bacteria, and around 200 isolated from plants (Diaz-Munoz, Miranda et al. 2018). They are also found in common foods such as peas, cabbages, lettuce, and beans. Their structure is derived from 9,10-anthracenedione, a quinone derivative of anthracene, whose basic three-ring structure can be modified by the addition of functional groups or other cyclic systems. This gives anthraquinones a range of colours, from red to blue in the base compounds, and from yellow-orange to brown in the derivatives (Fried, Oprea et al. 2022).

The solubility of anthraquinones depends on their structure and the functional groups present. In general, natural anthraquinone compounds tend to be soluble in water or polar solvents, due to the presence of hydroxyl or carboxyl groups, whereas synthetic anthraquinones are typically insoluble in water because of the presence of hydrophobic substituents (Diaz-Munoz, Miranda et al. 2018).

Historically known, as demonstrated by their discovery on mummy wrappings over 4,000 years old, anthraquinone pigments are especially valued in the textile field due to their brightness and remarkable lightfastness (Shen, Ren et al. 2023). The excellent fastness properties of anthraquinone dyes make them ideal for the textile industry, where they are used to dye cellulosic fibers through vat dyeing and synthetic fibers such as polyester, polyamide, and acetate via disperse dyeing (Fried, Oprea et al. 2022).

Beyond their use as dyes, anthraquinones exhibit numerous biological properties, including antitumor, anti-inflammatory, antifungal, antibacterial, and antioxidant activity (Diaz-Munoz, Miranda et al. 2018). Some anthraquinone pigments are also employed in agriculture for their repellent properties against insects and animals (Deliberto and Werner 2016).

Enviromental impact of the textile industry

Nowadays, the textile industry is considered one of the most polluting human activities due to its consumption of water resources, CO_2 emissions, chemical pollution, and textile waste. The fashion industry, in particular, uses enormous amounts of water (approximately 79 trillion liters per year) and contributes to around 20% of global water pollution due to dyes and other chemicals employed during processing, which are dispersed through textile wastewater (Niinimäki, Peters et al. 2020).

It is estimated that 10% of the chemicals used in textile production pose a high risk to human health, as they can spread globally and bioaccumulate, causing allergic reactions and increasing cancer risk (Posner and Jönsson 2014). Known as POPs (Persistent Organic Pollutants), these toxic substances resist degradation and accumulate in living organisms. They can spread extensively through natural processes involving soil, water, and air, reaching significantly high concentrations in the food chain and proving toxic to both humans and wildlife (Patra and Pariti 2022).

In 2011, the global NGO Greenpeace (www.greenpeace.org) published a report based on its investigations into wastewater discharges from two textile factories in China, revealing the presence of hazardous and persistent chemicals capable of causing hormonal disruption. One highly studied endocrine disruptor is nonylphenol, a surfactant that was restricted in 2021 under Regulation (EU) 2016/26. It can mimic estradiol, a female hormone, and thus affect the development, reproductive, neural, and immune systems of both humans and aquatic animals (Patra and Pariti 2022).

Chemicals used to waterproof fabrics, such as chemically stable fluoropolymers, have also been detected in the bodies of polar bears and seals in remote Arctic regions, demonstrating the global and persistent environmental impact of these substances (Niinimäki, Peters et al. 2020).

The textile industry, moreover, with an annual production of approximately 5 billion tons of CO_2, is responsible for 10% of global carbon dioxide emissions, considering the entire production cycle—from manufacturing to transportation (Niinimäki, Peters et al. 2020). Another significant issue is the constant increase in textile waste, which is estimated to amount to 92 million tons per year (Niinimäki, Peters et al. 2020). This waste is divided into pre-consumer waste, such as production scraps, and post-consumer waste, whose volume is steadily rising due to the fast fashion.

Pollution and release of chemicals by the textile industry

One of the main issues is the widespread use of toxic chemicals in various textile industry processes, which represents a significant obstacle to the sector's eco-compatibility, contributing to water pollution and making material recycling difficult. It is therefore essential to invest in the search for viable natural and eco-friendly alternatives in order to truly improve the environmental impact of the entire textile sector.

The textile industry uses over 8,000 chemical substances throughout the different stages of production—including dyeing, printing, bleaching, and finishing—to give fabrics vibrant colours, wash resistance, water repellency or stain resistance, and other functional characteristics. It is estimated that among the substances used solely for dyeing, about 72 have been identified as toxic, of which at least 30 cannot be treated (Kant 2012).

Synthetic pigments, although offering a wide colour range and high performance, are derived from non-renewable fossil sources such as petroleum and coal, making them

non-biodegradable and in some cases carcinogenic. Among the numerous classes of synthetic dyes developed, the most important are azo dyes, followed by anthraquinones and phthalocyanines (Fried, Oprea et al. 2022).

Azo dyes, which account for over 50% of all textile dyes used, are synthesized from aromatic hydrocarbons such as benzene, toluene, naphthalene, phenol, and aniline. Their structure is characterized by the presence of azo bonds (–N=N–), which, under reductive conditions, can be cleaved, releasing toxic aromatic amines known to be carcinogenic (Alsukaibi 2022).

Synthetic anthraquinones, composed of three condensed aromatic rings and also derived from benzene, allow for a wide variety of colour tones through modifications of their functional groups.

Phthalocyanines, on the other hand, are synthesized from phthalocyanuric acid or phthalic anhydride through high-temperature processes that promote the formation of metal complexes; however, high concentrations of metal ions resulting from the degradation processes of these molecules may exhibit toxic effects (Fried, Oprea et al. 2022). In absolute terms, up to 200,000 tons of synthetic dyes can be released into the environment each year due to the inefficiency of conventional wastewater treatment processes.

These substances, which are highly stable and non-biodegradable, persist in the environment, causing a series of negative consequences, including toxic effects on wildlife and an increase in water turbidity which, by limiting sunlight penetration, hinders the photosynthetic activity of aquatic plants (Kant 2012).

The lack of photosynthesis leads to a decrease in oxygen production, causing hypoxia—a phenomenon that reduces dissolved oxygen levels in water and puts aquatic life at risk (Kant 2012). This pollution, in addition to damaging natural ecosystems, also limits the usability of water resources by making the contaminated water unsuitable for human consumption and agricultural irrigation (Kant 2012).

Current and possible applications of anthraquinones.

Anthraquinones are the most abundant class of natural quinones, with around 700 compounds being reported 200 obtained from plants; their structure allows them to carry out activities in different areas with a wide range of applications (Diaz-Munoz, Miranda et al. 2018).

Historically Anthraquinone-containing plants, such as, aloe vera and rhubarb, have been known and used for in, for the treatment of health problems such as skin ailments and constipation (Zari and Zari 2015, Neyrinck, Rodriguez et al. 2022, Yang, Wan et al. 2022). Laxative anthraquinones are usually taken in their glycosylated form, these compounds bypass hydrolysis in the stomach and the action of α-glucosidase enzymes in the small intestine to arrive unchanged in the large intestine where reductive cleavage of the sugar moiety by bacterial β-glucosidases and reductases converts them into the

corresponding pharmacologically active aglycones (Malik and Müller 2016). For example, Aloin A an active compound contained in aloe vera, was found to decompose into aloe-emodin and aloe-emodin-9-anthrone, the latter was found to inhibit colonic Na+/K+-ATPase, causing water retention in the intestinal lumen (Malik and Müller 2016).

Beside their known laxative functions, there has been a growing interest in the application of anthraquinones and understanding their clinical mode of action in different fields of medicine. As an example, starting from the discovery of Daunorubicin isolated from *Streptomyces peucetius* (Di Marco, Cassinelli et al. 1981), other five related compounds have been approved for clinical use thanks to their anticancer properties (Minotti, Menna et al. 2004). The main target appears to be the enzyme topoisomerase II, where they stabilize and block the enzyme in the "cleavage complex" configuration, leading to DNA damage and fragmentation (Nitiss 2009, Wu, Li et al. 2013).

More recently many natural anthraquinones have been screened for different properties, for example anthraquinone glycosides obtained from *Cassia obtusifolia* seeds have been shown to possess hepatoprotective properties (Paudel, Jung et al. 2018) as well as five Rumabynosides, obtained from the rhizomes of *Rumex abyssinicus* showed hepatoprotective potential against CCl4 induced damage (Lonkeng, Eckhardt et al. 2024). Among others, many applications for anthraquinones continue to be explored such as, antimalarial (Hou, Cao et al. 2009, Patel, Beteck et al. 2021), antimicrobial (Xiang, Song et al. 2008, Malmir, Serrano et al. 2017, Raghuveer, Pai et al. 2023), antiviral (Semple, Pyke et al. 2001) and antioxidant (Marković, Jeremić et al. 2016).

Looking further than clinical applications, natural and synthetic anthraquinones have found use in a variety of different technological fields. One of the most prominent is the textile industry; here natural anthraquinone dyes were employed under the form of plant extracts from plants such as *robia tinctorium* (De Santis and Moresi 2007). After the synthesis of mauveine an increasing number synthetic pigments have been developed and substituted naturally sourced pigments, as their production remained constant over the year and resulted in lower costs.

Beside textile fibres, anthraquinones demonstrated their compatibility as additives, to building materials and paints, where they prevent degradation by pests (Ballinger Jr 2015), inside this line of research, the use of anthraquinones can be implemented for inhibition of biofilm formation, substituting current chemicals with natural secondary metabolites (Qiu, Gu et al. 2024). when compared to currently used additives, microbially derived anthraquinones showed comparable or increased performances, against marine biofilm forming bacteria (Preet, Gomez-Banderas et al. 2022) and against clinically relevant biofilm forming bacteria (Prateeksha, Bajpai et al. 2021). Anthraquinones are also being explored for the development of sensors (Khankaew,

Mills et al. 2017), implementation into batteries (Fontmorin, Guiheneuf et al. 2022), and agricultural crop protection (Deliberto and Werner 2016).

Objectives

Collectively the general objective of this research was to identify and characterise pigmented microorganisms from under-explored environments as potential producers of bioactive natural compounds, with particular interest on pigments and additional metabolites of biotechnological relevance. This work aimed to develop and validate an integrated discovery pipeline that combines classical microbiological approaches with advanced analytical and genomic methodologies for the systematic identification of biologically active natural compound (BNC) producers.

The first objective was to implement a targeted isolation strategy to recover pigmented strains and to select promising candidates based on pigmentation characteristics, growth performance, and scalability. Selected isolates were subjected to standardized fermentation and solvent extraction procedures to obtain metabolite-rich fractions suitable for chemical and functional analyses.

The second objective was to characterise the metabolic profiles of these isolates using ultra-performance liquid chromatography–mass spectrometry (UPLC–MS), enabling detection and comparative assessment of pigment-related compounds, including anthraquinones and carotenoids. Together whole-genome sequencing and biosynthetic gene cluster (BGC) mining were performed to evaluate the genomic potential for secondary metabolite production. Predicted terpene, polyketide synthase (PKS), and non-ribosomal peptide synthetase (NRPS) clusters were analysed and, where possible, correlated with observed metabolomic signatures.

The last objective was to assess the biological activity of extracts through functional screening, including total antioxidant capacity, antimicrobial assays, and antibiofilm activity. This multi-assay approach enabled evaluation of functional potential across different activity models.

These objectives were aimed for, in order to establish a reproducible and scalable workflow integrating microbial isolation, fermentation, extraction, metabolomic profiling, genome mining, and functional screening. The resulting framework provides a structured strategy for the discovery and preliminary characterisation of novel pigment-producing and bioactive microorganisms, while laying the foundation for future optimisation and biotechnological exploitation.

MATERIALS AND METHODS

Selection of environments and Preparation of culture Media

To isolate the microorganisms, present in the collected samples, an exploratory approach combined with a literature review was adopted in order to increase the likelihood of isolating pigmented organisms. To support the growth of a wide spectrum of microorganisms, both rich and minimal media were used.

The selected rich media included: Tryptone Soy Agar (TSA) (Song, Song et al. 2017), a highly versatile medium with a large quantity of nutrients that supports the growth of a wide range of bacteria and yeasts and was primarily used during the isolation of microorganisms not hailing from sea environments. On the contrary for samples from marine environments, Marine Agar (MA) (Devi, Rajendran et al. 2011, Moore, Robson et al. 2020) was used, a rich complex medium designed for the cultivation of marine microorganisms that often require a higher salinity to thrive. As a minimal defined substrate, Vogel's medium N (Vogel) (Vogel 1956, Moore, Robson et al. 2020) was used during the isolation of microorganisms from Presena glacier and Volcano marine sediments; it provides limited nutrients in the form of glucose and mineral salts, without the presence of amino acids or vitamins, thus restricting growth to only microorganisms with capabilities for oligotrophy.

For the isolation of microorganisms form coral samples additional minimal media were tested: Chemosynthetic Z (CZ) and Chemosynthetic N (CN), both defined minimal media specifically designed for the isolation of chemoautotrophic microorganisms capable of utilizing sulphur (CZ) or fixing nitrogen (CN), these media were employed. These were adapted from media found in the literature (Wada, Shoda et al. 1986, Distel, Altamia et al. 2017). For each type of medium, Petri dishes were prepared containing 20 ml of agarized medium, on which the target microorganisms were cultivated.

Sampling and Microorganism Isolation Methods

Some samples were collected directly by our research group, while others were provided through collaborations. Upon arrival at the laboratory, the samples were processed according to their type, aiming to isolate the widest possible diversity of pigmented microorganisms.

Snow – Presena Glacier, Trentino-Alto Adige, Italy Snow was collected in sterile two-litre bottles using gloves and sterile tools. The sample was melted at 4 °C, and the resulting water was centrifuged in a 500 mL centrifuge bottle at 9000 g for 5 minutes (Beckman J2-HS). The supernatant was discarded and the pellet was resuspended in 10 mL of sterile water. 100 µL of the resuspended pellet were plated on TSA and Vogel's medium N. Plates were incubated at 18 °C and single colonies of interest were subsequently picked and propagated (Mortazavi, Hayes et al. 2008, Mortazavi, Attiya et al. 2014).

Cryoconite Holes – Brenta Glacier, Italy & Svínafellsjökull Glacier, Iceland Cryoconite samples, collected in 50 mL Falcon tubes, were centrifuged at 9000 g for 5 minutes. The supernatant was removed, and 1 g of cryoconite pellet was resuspended in 10 mL of sterile saline solution. Samples were agitated for 30 minutes at 140 RPM and serially diluted tenfold. 100 µL of each dilution were plated on TSA and Vogel's medium N agar. All plates were incubated at 12 °C, and single colonies of interest were selected for propagation (Christner, Kvitko et al. 2003, Margesin, Schumann et al. 2012).

Fallen Leaves – Valpiana, Trentino-Alto Adige, Italy Leaves showing signs of microbial activity—evident through dark spots—were collected. Each leaf was cut, using sterile instruments, into square pieces of with an area of approximately 4 cm^2 and placed directly on TSA and Vogel's medium N plates for 10 minutes to facilitate microbial transfer. Leaf pieces were then removed, and plates were incubated at 18 °C. Colonies of interest were subsequently isolated and propagated (Yashiro, Spear et al. 2011, Lu, Han et al. 2022).

Boat Hull Sediments – Rimini, Emilia-Romagna, Italy Mouldy patches found on boat hulls were sampled using swabs. These swabs were streaked directly onto Marine Agar and Vogel's medium N plates. Plates were incubated at 25 °C, and selected colonies were picked and further propagated.

Marine Sediments – Vulcano, Sicily, Italy Marine sediment samples were provided in three 15 mL Falcon tubes. 1 g of sediment from each tube was serially diluted in artificial seawater (ASW), and 100 µL of each dilution were plated on TSA, MA, and Vogel's medium N agar (Romanenko, Otstavnykh et al. 2023). Plates were incubated at 22 °C, and colonies of interest were selected for propagation (Radovanović, Milutinović et al. 2018, Romanenko, Otstavnykh et al. 2023).

Corals and Seagrass – Panarea, Sicily, Italy Four coral species were sampled in two sites: Near gas emissions (Vent): *Balanophyllia europaea*, *Caryophyllia inornata* in three colour variants (pink, brown, white). And away from emissions (No Vent): *Balanophyllia europaea*, *Astroides calycularis* (orange), *Leptosammia pruvoti* (yellow) In both sites, samples of *Posidonia oceanica* were also collected. Small clusters of polyps still connected by their skeleton were harvested. Individual polyps were separated and

cleaned of algae using sterile tweezers and scalpels. Surface sterilization was performed in three steps: rinsing in sterile ASW, immersion in 70% ethanol for 3 seconds, and a final rinse in sterile ASW. This eliminated surface microorganisms not relevant to the study, as coral symbionts inhabit the gastric cavity (coelenteron). After sterilization, a single polyp was ground using a mortar and pestle to obtain a homogeneous mass, which was serially diluted in six glass tubes, each containing 9 mL of ASW (Palladino, Caroselli et al. 2022). The same protocol, minus the sterilization steps, was applied to *Posidonia oceanica* samples. These were mechanically fragmented and diluted as described. 100 µL of each dilution were plated on TSA, MA, Vogel's medium N, CN, and CZ media. Plates were incubated at 25 °C. TSA, MA, and Vogel plates were incubated aerobically, while CN and CZ were incubated under micro-aerophilic conditions using Anaerocult gas packs (Millipore) in 2.5 L jars. Colonies of interest were subsequently picked and propagated (Susilowati, Ardianti et al. 2021, Wang, Liu et al. 2022). For microorganisms isolated on CN and CZ media, after propagation in sterile culture, one colony was transferred to MA and TSA plates to assess their growth under aerobic conditions and on richer media. Remaining colonies were scraped and preserved as glycerol stocks. All organisms isolated on CN and CZ were capable of growth under aerobic conditions on complex media.

Growth, Propagation, and Initial colour Screening

Plate growth was monitored daily, with colour screening performed approximately every two days across all plates—from cultures containing mixed microbial communities (-1) to the highest dilution levels (-6). Coloured colonies of interest were selected and propagated in an attempt to isolate the microorganisms. For the most promising colonies exhibiting intense pigmentation, propagation was repeated multiple times until pure cultures of the target isolate were obtained.

Glycerol Stock Preservation and DNA Extraction

From the pure cultures, a single pigmented colony was collected using a sterile loop from solid medium and inoculated into 250 mL Erlenmeyer flasks containing 25 mL of liquid medium corresponding to the same solid media used for extraction. The flasks were incubated in a shaking incubator at 25 °C and 100 rpm and allowed to grow for 72 or 96 hours. Upon reaching the stationary growth phase, the microorganisms underwent morphological evaluation using an optical microscope (ZEISS) to distinguish bacterial samples from fungal ones. The culture broth was then transferred into two 15 mL Falcon tubes and centrifuged at 9000 g for 5 minutes (Beckman J2-HS), to collect cell pellets for both molecular characterization and long-term preservation via glycerol stocks.

For glycerol stock preparation, half of each cell pellet was resuspended in 2 mL of fresh growth medium supplemented with 10% glycerol and stored in 2 mL cryovials at –80 °C. For molecular identification, DNA was extracted from the remaining cell pellets using the DNeasy Blood & Tissue Kit (QIAGEN) and quantified using a NanoDrop ND-1000 spectrophotometer (NanoDrop Technologies, Wilmington, DE, USA).

A marker gene approach was then applied: PCR amplification targeted the bacterial 16S rRNA gene and the ITS regions of yeasts. Sequencing was performed via Sanger sequencing by Biofab Research (Rome, Italy).

Bioinformatic Analysis and Taxonomic Identification

The sequencing data received were visualized using Teal (Rausch, Fritz et al. 2020) (Teal: Trace Analysis Viewer | GEAR, [www.gear-genomics.com/teal/]), a bioinformatics tool useful for examining sequencing outputs and reading files in ".fasta" format. Teal generates an electropherogram—a graph where the x-axis represents curves for individual nucleotides and the y-axis displays the signal amplitude—allowing evaluation of the sequencing quality.

The nucleotide sequences visualized were manually cleaned by trimming low-quality regions, ensuring that subsequent analyses were performed only on high-quality reads. The validated reads were then aligned against the rRNA/ITS databases using the Nucleotide BLAST platform (Altschul, Gish et al. 1990) (BLAST: Basic Local Alignment Search Tool, (https://blast.ncbi.nlm.nih.gov/Blast.cgi). BLAST is an optimized algorithm for comparing sequences efficiently and identifying the best local alignments against database entries (NCBI BLAST documentation).

Each BLAST run recorded the following key information: Full name of the microorganism whose 16S or ITS gene alignment showed the greatest similarity to the query sequence Query Coverage – the percentage of the input sequence covered by the aligned database sequence Percentage Identity – the percentage of nucleotides that were exactly identical between the query and the database match E-value – a statistical measure indicating the significance of the alignment between the original sequence and the query. To ensure reliable taxonomic identification, results were selected based on high Query Coverage and Percentage Identity values (preferably >95%), along with minimal E-values close to zero.

Absorbance at 600 nm

To quantify the cellular growth and density reached by the different strains, absorbance at 600 nm was measured, this wavelength allows us to estimate the number of cells in suspension, thus acting as a proxy of the cellular density reached in stationary phase.

To perform the measurement, each strain was cultured in 10 mL of liquid medium, using Tryptone Soy Broth (TSB) or Marine Broth (MB) depending on media employed during the isolation phases, then once stationary phase was reached, 1 mL of culture broth was transferred into a cuvette and analysed using a spectrophotometer. If the absorbance value exceeded 1, the sample was diluted with fresh culture medium and the measurement repeated to obtain a more accurate signal, both absorption value and dilution factor were recorded, all strains were incubated at 25 °C.

Evaluation and Cataloguing of Pigmentation in Isolated Strains

Each strain was cultured in a 250 mL Erlenmeyer flask containing 20 mL of rich liquid medium, using Tryptone Soy Broth (TSB) or Marine Broth (MB) depending on the growth capabilities demonstrated during preliminary phases.

Upon reaching the stationary phase—typically between 72 and 96 hours of incubation—the cell broth of each strain was photographed under natural light. It was then transferred into 15 mL Falcon tubes and centrifuged at 9000 g for 5 minutes using a Beckman J2-HS centrifuge. The resulting cell pellet was also photographed under natural

light to document chromatic variations between the liquid culture and the pellet. To enhance image contrast, all photographs were taken against a solid black or white background.

Selection of candidate strains to further characterize

All identified strains underwent a screening process, with the goal of selecting the most promising candidates for subsequent steps involving growth optimization, scale-up, and chemical characterization.

The screening process was conducted at their stationary growth phase, considering parameters such as colorimetric properties, light absorbance at 600 nm, and compatibility with cost-effective and readily available culture substrates.

This approach, ultimately led to the selection of seven candidate strains: *Rhodosporidiobolus colostri* (MT6), *Cytobacillus oceanisediminis* (MT14), *Alkhalihalobacillus algicola* (MT8), *Planococcus glacei* (MT37), *Paracoccus marcusii* (MT26) *Cladosporium* sp (MT27) and *Micrococcus yunnanensis* (MT16).

Characterization of selected strains, Growth Curves:

Growth curves were constructed for the seven selected strains as part of their in depth characterization. Starter culture were prepared for each strain in a 250 mL Erlenmeyer flask containing 25 mL of liquid medium, inoculated from a glycerol stock. After 24 hours of incubation, 100 µL of the starter culture was transferred into a flask containing 30 mL of the selected test media and incubated for 34 hours while monitoring changes in absorbance. TSB medium was chosen for *Micrococcus yunnannensis, Rhodosporidiobolus colostri* and *Bacillus* oceanosediminis, while MB was employed for *Alkhalihalobacillus algicola, Planococcus glacei, Paracoccus marcusii* and *Cladosporium* sp. Strains were incubated at 20 °C, 25°C or 30 °C depending on the optimum growth temperature reported in literature for other strains of the same species. At regular intervals, every two hours, optical density at 600 nm was measured using a spectrophotometer. If absorbance values exceeded 1, samples were diluted with fresh culture medium, remeasured, and the dilution factor was recorded. At the end of the measurement period, corrected absorbance values were calculated by multiplying the measured absorbance by the dilution factor (Equation 1).

$$ABSt = MABSt \cdot DFt$$

Equation 1: The corrected absorbance values for each time point (ABSt) are calculated by multiplying the measured absorbance (MABSt) by the dilution factor (DFt) used at the time (t) of measurement.

To model bacterial growth, corrected absorbance values and corresponding time points were fitted to the logistic equation (Equation 2) using the R software environment (R Core Team, http://www.r-project.org) and the packages “growthcurver” (https://cran.r project.org/web/packages/growthcurver) (Sprouffske and Wagner 2016) and “gridExtra” (https://cran.r project.org/web/packages/gridExtra).

$$Nt = \frac{(K)}{1 + \left(\frac{K - N0}{N0}\right) e^{-rt}}$$

Equation 2: General formula of the logistic equation, this equation can be used to model the growth of a population of microorganisms, Nt represents the population at point t, K is the carrying capacity, which is the maximum population value that can be reached under the conditions studied, r is the intrinsic growth rate, meaning the maximum growth rate, that can be reached under the conditions studied, and t represents time.

Characterization of selected strains, Carbohydrate's metabolism:

The ability of each strain to utilize different carbon sources was evaluated using API 50 CH strips (Biomerieux, Marcy-l'Étoile, France). Each strain was evaluated twice, once in aerobic conditions while the second time in anaerobic conditions.

For evaluation in aerobic conditions, the strips were employed according to the manufacturer instructions, the tray present in the kit was labelled and lined with water to maintain humidity, then for each of the strains to be characterized, a single colony was scooped using a loop and mixed with the provided CBH/E growth media to obtain a homogenous cell suspension, this suspension was later inoculated in each cupule of the strips in the same amount and finally the tray was closed with a lid present in the kit and incubated at 25 °C for two days.

The same process was employed for the evaluation in anaerobic conditions with a single difference, after an API kit had been inoculated with a cell suspension, each of the cupule was sealed using three drops of mineral oil, to avoid the solubilisation of environmental O_2 in the culture media.

The kits were then monitored over the course of two days after 24 and 48 hours, as per producer's instructions, and each change of colour in the media was recorded.

Characterization of selected strains, Genome sequencing, Phylogeny reconstruction and BGCs Prediction:

The next step of characterization for each of our strains was to obtain their complete genome through sequencing, to do so biomass samples for each of our strain were processed using commercial kits from QIAGEN, for DNA extraction, library preparation and paired end sequencing. In particular, cell pellets for each of the selected strains were subjected to DNA extraction using the DNeasy Blood & Tissue Kit (QIAGEN) and quantified using a NanoDrop ND-1000 spectrophotometer (NanoDrop Technologies, Wilmington, DE, USA). Subsequently, each DNA sample was further purified with 1.8× AMPure XP beads to remove inhibitory compounds such as salts and chelants, following clean-up, DNA concentration was quantified using a Qubit dsDNA assay. Next, library preparation had been carried out using the QIAseq FX DNA Library Kit (QIAGEN) following manufacturer's instructions. Briefly, input DNA was enzymatically fragmented at 32 °C for 10 minutes, using the FX DNA Enzyme Mix, for samples containing more than 100 ng of input DNA. While for samples containing less than 10 ng of DNA, fragmentation lasted 16 minutes at 32 °C. Immediately following fragmentation, end-repair and A-

tailing were also performed in the same reaction mixture, using a thermocycler, following manufactures suggested incubation times. Next adapters were ligated to each sample of fragmented DNA, by adding 45 µl of ligation master mix to 55 µl of sample and incubating at 20 °C for 15 minutes. Ligated DNA was than purified using AMPure XP beads. After clean-up, samples were PCR-amplified and finally, libraries were pooled equimolarly into a single tube and subjected to Illumina sequencing.

Following genome sequencing, raw paired-end reads obtained were processed within a work pipeline composed of specialized bioinformatic tools, in order to reconstruct the continuous genome of our strains and to mine it for the presence of Biosynthetic gene clusters. Raw paired-end reads obtained from Illumina sequencing were initially processed with fastp (v.0.20.1) a tool that allows for the fast processing and quality check of data in FastQ format. Using fastp the following steps were performed; detection and removal of sequencing adapters (--detect_adapter_for_pe), trimming of low-quality bases at the ends of reads (--cut_tail), a quality-based filtering (-c) and finally the removal of duplicated reads (-D). this ensured the production of a high-quality dataset for downstream analyses by reducing sequencing artifacts and technical noise. The now filtered reads were then assembled de novo with Unicycler (v.0.5.0) (Wick, Judd et al. 2017), to maximize contig bridging and completeness of the assemblies, bold mode was selected, resulting assemblies produced in FASTA format, contained scaffolds and contigs representing draft genomes. Next, the assembly quality and reliability were evaluated using QUAST (v.5.0.2) in which both assemblies and corresponding filtered reads were fed to the tool as input, for the estimation of key assembly statistics such as N50, L50, total assembly length, number of contigs, and GC content. QUAST also compared the assemblies against raw data to assess potential misassembles artefacts and evaluate the degree of completeness. After quality evaluation of the reconstructed genomes, the correct taxonomic placement of each strain was evaluated by using GTDB-Tk (v.2.1.1) (Quast, Pruesse et al. 2012), by applying the classify_wf workflow against the Genome Taxonomy Database (GTDB).

For the phylogeny analysis and genome annotation of our strains, publicly available genomes belonging to the strains genera were retrieved from the NCBI RefSeq database using the NCBI Datasets command-line tool. To ensure high assembly quality and minimize biases associated with fragmented genomes, only assemblies of complete genome or chromosome-level assemblies were included in the dataset. Downloaded genome packages were extracted locally and organized into FASTA format, all bioinformatic analyses were conducted within Conda-managed environments to ensure reproducibility and strict control of software dependencies. To eliminate redundancy and retain representative genomes, a dereplication was performed using dRep (Olm, Brown et al. 2017). Genome assemblies were evaluated based on completeness and contamination metrics, retaining only those with ≥90% completeness and ≤5% contamination. Followingly dereplication was performed using a two-step Average Nucleotide Identity (ANI)-based clustering approach. A primary clustering threshold of 90% ANI was applied to group distantly related genomes, followed by a more stringent secondary clustering threshold of 99% ANI to collapse nearly identical strains. Dendrograms representing genomic similarity among strains of interest and related microrganisms were than produced based on ANI values.

Identification of secondary metabolite biosynthetic potential was carried out with antiSMASH (v.6.0) (Blin, Shaw et al. 2023). which included comparison of identified BGCS against the MIBiG reference database of known biosynthetic gene clusters, detection of subclusters, and gene annotation with Prodigal. Hidden Markov model search (--fullhmmer) was employed to refine the identification of conserved motifs within biosynthetic domains. The final outputs of antiSMASH consisted of interactive HTML reports, that enabled the visualization and characterization of putative biosynthetic gene clusters (BGCs) within the genomes under study. Than antiSMASH output was analysed using PRISM (Skinnider, Johnston et al. 2020) to predict the structure of possible BNC products, when this ielded a viable structure, it was then visualized using PubChem Sketcher.

Characterization of selected strains, Chemical characterization:

The last steps of strain characterization had the goal of characterizing the chemical profile of metabolites produced by each strain in particular, focusing on pigmented compounds.

Production of biomass

In order to have the necessary biomass to proceed with extractions of pigments, each strain was grown using one 5 L Applikon fermenter, filled with 3 L of liquid media, the conditions and media used were based on performances obtained, by each strain, during evaluation of culture growth.

Starting from *Rhodosporidiobolus colostri* (MT6), during fermentation, temperature was set at 20°C, pH was kept at 7, air influx was set to 1 PPV with a constant stirring speed of 450, TSB was used as the growth media. Tryptone soya broth was also used for the fermentation of *Cytobacillus oceanisediminis* (MT14, RAM20), temperature was maintained at 30°C, pH at 7, stirring speed was kept constant at 400 RPM and air influx was set to 1 PPV. Meanwhile for the fermentation of *Alkhalihalobacillus algicola* (MT8, RAZ4) the media used was: Marine broth, temperature was maintained at 25°C, pH at 7, stirring speed was kept constant at 450 RPM and air influx was set to 1 PPV. *Planococcus glacei* (MT37, MA CIR (VENT) (-3) X.5), was fermented in Marine broth, the temperature was maintained at 25°C, pH at 7, stirring speed was kept constant at 450 RPM and air influx was set to 1 PPV. *Paracoccus marcusii* (MT26, MA POS (NV) (-1) O) was fermented in Marine broth, the temperature was maintained at 25°C, pH at 7, stirring speed was kept constant at 450 RPM and air influx was set to 1 PPV. and *Cladosporium* sp. (MT27, MA CIB (VENT) (CN -5) ·) was also fermented in Marine broth, the temperature was maintained at 25°C, pH at 7, stirring speed was kept constant at 400 RPM and air influx was set to 1 PPV. Lastly for *Micrococcus yunnanensis* (MT16, RAZ24), the media used was: Tryptone soya broth, temperature was maintained at 30°C, pH at 7, stirring speed was kept constant at 420 RPM and air influx was set to 1 PPV. Fermentation lasted 72 hours for all strains, allowing for the development of deep colouration and production of secondary metabolites during stationary growth phase. After fermentation was completed the resulting broths were retrieved from the Applikon bioreactor,

centrifuged at 9000 x g for 5 minutes in a Beckman J2-HS centrifuge using 500 mL Beckman centrifuge bottles (Beckman, Brea, California), and the pigmented cell mass was retrieved, the clear supernatant were decanted, except for strains: *Paracoccus marcusii* (MT26) and *Cladosporium* sp. (MT27), which were saved for later characterization as they presented a change in colour due to the production and release of a water soluble pigment after fermentation.

Then to proceed with the crude extraction of pigments the cell mass of each strain was weighted (wet weight), each gram of cells was resuspended in 3 mL of distilled water and lysed via sonication using a Branson sonifier 250 equipped with a ½" titanium disruptor horn (Branson, Brookfield, Connecticut).

In particular, bacterial strain have been lysed in a refrigerated bath, with 6 cycles of sonication at output 7 and duty cycle 80%, each cycle lasted 2 minutes with 1 minute of pause between each (Patchett, Neal et al. 1989, Burgess 1996, Wingfield 2005). While fungal strains where lysed in a refrigerated bath, with 3 cycles of sonication at output 9 and duty cycle 90%, each cycle lasted 15 minutes with 15 minutes of pause between each (Wu, Yu et al. 2015, Patel, Arora et al. 2019).

Extraction of biomass

Later a method for the extraction of pigments and anthraquinone like molecules from cell pellets, was developed based on direct liquid extraction techniques found in literature (Lech and Jarosz 2011, Barrera Vázquez, Comini et al. 2014, Shi, Li et al. 2014, Duval, Pecher et al. 2016, Patel, Arora et al. 2019, Chia, Chew et al. 2020, Gurkok 2022), in this context 3mL aliquots of crude extract, 6mL of water and 9mL of hexane were added together into a single tube, the mixture was than shake vigorously in a vortex for 2 minutes to allow homogenous phase contact of cell components with both the water and organic phase, aliquots were than sonicated in a sonicating bath for 15 minutes and then centrifuged at 20000 g for 5 minutes. At the end of centrifugation, both water and hexane were removed, while the cell pellets were kept and 12mL of solvent mixture ACN:MetOH (5:2) were added to them, the samples were vortexed again for at least 2 minutes to ensure the resuspension of cell components, then samples were sonicated in a sonicating bath for 1 hour. At the end of the sonicating bath samples were centrifuged at 20000 g for 5 minutes and the supernatant is filtered through filter paper, to ensure that the colourless cell debris are removed from the now pigmented organic phase. Lastly the pigmented extract is rota evaporated at 60°C at -3 bar pressure to reduce the volume of sample from 12 mL to 1 mL, the sample was then saved in a HPLC compatible vial.

While for samples of cell free broths (CFB) obtained from the strains *P. marcusii* (MT26) and *Cladosporium* (MT27) a different protocol was developed based on techniques found in literature (Shi, Li et al. 2014, Duval, Pecher et al. 2016, Patel, Arora et al. 2019),here 10 mL of CFB sample were added to 90 mL of ethanol and mixed thoroughly, the mixture was let to rest for 5 minutes and subsequently centrifuged at 20000 g for 5 minutes, resulting in the formation of two phases, a clear and pigmented supernatant, and a cloudy precipitate, the supernatant was retrieved while the precipitate was discarded, to make sure the supernatant did not contain any residual precipitate, it was

filtered through filter paper and collected in a balloon flask. After filtration, the sample had been rota evaporated at 60°C at -3 bar pressure and resuspended in 1 mL of distilled water, the sample was then saved in a HPLC compatible vial.

HPLC-UV/VIS analysis

The absorption spectra of the samples obtained from these extraction procedures were then analysed through the use of a HPLC-UV/VIS equipped with a C18 column (150 mm × 4.6 mm, 5 µm) and a set measuring wavelength range of 450 nm, and. The mobile phases chosen were water (Phase A) and a mixture of Acetonitrile:Acetone 3:1 (Phase B) using the following elution gradient: 0 - 4 min: 10% B, 4 - 7.5 min: 10-20% B, 7.5 - 10 min: 20-40% B, 10 - 12 min: 40% B , 12 - 15 min: 40-70% B, 15 - 20 min: 70% B, 20 - 25 min: 70-90% B, 25 - 30 min: 90% B, 30 - 45 min: 90-97% B, 45 - 60 min: 97% B and finally a post-run: 10% B for 5 minutes. The flow rate was set at 0.6 mL/min with an injection volume of 10 uL and a column temperature of 25°C. Samples obtained from extractions were injected alongside multiple solutions of AQs molecular standards (Emodin, Aloe-emodin, Quinizarin, Rhein, Carminic acid, Physcion) at different concentrations in order to obtain calibration curves and quantify possible AQs molecules present in our sample.

UPLC-MS analysis

The mass spectra of the samples were also analysed through the use of a UPLC-MS machine, equipped with a time-of-flight Mass detector (Waters G2-XS QTof-MS) (Milford, Massachusetts, U.S.). Analysis were performed in ESI- mode, the column used was Acuity UPLC BEH C18 1,7um 2,1x100 mm, mobile phases used were water+0.5% NH4OH (Phase A) and MeOH+0.5% NH4OH (Phase B), employed along a gradient elutions following these steps: 0 - 3 min: 5% B, 3 - 6 min: 25% B, 6 - 10 min: 25% B, 10 - 16 min: 66% B, 16 - 20 min: 100% B, 20 - 21 min: 5% B. Flow rate was kept at 0.3 ml/min with an injection volume of 10 µL. Samples obtained from extractions were injected alongside multiple solutions of AQs internal standards (Emodin, Aloe-emodin, Quinizarin, Rhein, Carminic acid, Physcion) at different concentrations in order to obtain calibration curves and quantify possible AQs molecules present in our sample. Measurements and values for the presence of AQs in both our samples and standard solutions were taken in Extract Ion Mode, in order to have better visualization and more precise signal measurement for the mass-to-charge ratios (m/z) of the investigated anthraquinones.

Later, from the mass chromatograms obtained from our samples, the m/z ratios of other compounds different from anthraquinones were also investigated, to assess their possible presence inside the samples, and broadly characterize the chemical profile of produced compounds. The metabolites to be investigated were chosen from literature based on the production capabilities of each of our strains of interest.

Functional characterization of the extracts:

Antioxidant activity

To obtain information over the activity of molecules found inside the extracts we produced, a series of assays was performed.

Total antioxidant capacity (TAC) was measured employing a commercially available Antioxidant Assay Kit (Antioxidant assay kit, MAK334, Sigma-Aldrich), the assay is based on reduction of Cu^{2+} to Cu^{+} by antioxidants and formation of a Cu^{+}–dye complex that can be measured by reading Light absorbance at 570 nm. Kit was employed following manufacturers indications, briefly; 20 µL of samples and Trolox standard solutions were dispensed in separate wells of a clear flat-bottom 96-well plates, then 100 µL of reaction mix as provided by the kit, was added to each well. The plate was finally mixed and incubated for 10 min at room temperature, and absorbance read at 570 nm. Solvents samples were included as control.

After incubation a standard linearity curve was constructed using Absorbance values of Trolox solutions and the Total Antioxidant Capacity (TAC) of samples was calculated employing the equation reported below.

$$TAC\ (\mu M\ Trolox\ eq.) = \frac{(A_{570})_{sample} - (A_{570})_{blank}}{slope\ (\Delta A_{570}/\mu M)} \times dilution\ factor.$$

Equation 3: Equation used to obtain antioxidant power of the extracts, expressed as a concentration of Trolox solution of same the efficacy.

Antimicrobial activity

Later the antibiosis of seven different test strains was evaluated against three indicator bacterial strains, *Escherichia coli* CECT416, *Staphylococcus aureus*, and *Pseudomonas aeruginosa* T17E4. Using a cross-streak assay (Chemoh, Bin-Ismail et al. 2021, Silva, Paula et al. 2022).

Circular agar plates were prepared and seeded with one test strain each, by streaking the plate near the border, roughly for one third of the total area, plates were then incubated for two days to allow for the production and diffusion of compounds, following the plates were then retrieved and seeded with the indicator strains by streaking three lines perpendicularly to the test strains and once again incubated for 2 days. At the end of the second incubation period the plates were retrieved and inhibition of strain growth near contact point of the streaks was evaluated.

Finally, the antimicrobial activity of the extracts was also evaluated in liquid cultures (Ceruso, Clement et al. 2020, Aydemir, Odabaş Köse et al. 2024). The extracts employed for this antimicrobial assay were prepared from cell biomass of Micrococcus yunnannensis and *Paracoccus marcusii*. Acetone served as solvent control.

Liquid cultures of the three indicator strains were prepared the day before the assay and incubated at 37 °C overnight, the following day the grown cultures were diluted with fresh TSB media in order to obtain inoculums with an optical density of OD_{600} = 0.1.

Assay was assembled in a 24-well plate, each well contained 1.8 mL of the target indicator strain inoculum, plus 200 µL of extract to be tested, in two different concentrations: diluted 1/10 and undiluted, giving a final test volume of 2.0 mL per well. Wells for positive and negative controls were also prepared, positive control consisted

of 2.0 mL of inoculum at OD_{600} = 0.1 while negative control was composed only of sterile medium 2.0 mL; solvent controls were also prepared, the same way as samples, with matching dilutions of acetone.

Plate was then incubated overnight using a Varioskan lux plate reader (Thermo scientific), which allowed to incubate the plate at 37 *C as well as measure the Optical density continuously throughout the incubation.

Antimicrobial activity

Lastly the antibiofilm potential of four extracts was evaluated against the biofilm forming strain, *Pseudomonas aeruginosa* T17E4, using 96-well plate with a crystal-violet based assay (O'Toole 2011, Alam, Al Farraj et al. 2020). Extract evaluated were: *R. colostri* organic, *M. yunnanensis* organic, *P. marcusii* CFB 1:2 and *Cladosporium* CFB H_2O F2. For the whole duration of the assay, *Pseudomonas aeruginosa* T17E4 has been cultivated in TSB, at 37°C. Samples of Acetone and water were also employed as solvent controls.

Starting from a liquid culture of *Pseudomonas aeruginosa* T17E4, 10% inoculum was produced with new TSB, subsequently 100 µL of the 10% inoculum were added to each test well plus 100 µL of the extract to be tested. Solvent controls and solvent blanks were added, by pipetting 100 µL of solvent and 100 µL of 10% inoculum or 100 µL of fresh media respectively. Lastly a positive control made by pipetting 100 µL of inoculum and 100 µL of fresh medium and a negative control prepared by pipetting 200 µL of sterile medium only, were also added. Plates were then incubated statically at 37 °C to allow biofilm formation.

Subsequently, after 24 hours of incubation, 100 µL of sample was gently removed from each well without disturbing the biofilm, then transferred to a fresh plate and OD_{600} was measured to quantify planktonic growth.

Then each well of the original plate was carefully emptied of the remaining liquid sample without disturbing the biofilm, washed three times with 200 µL sterile PBS dispensed to the side of each well to avoid dislodging the biofilm, and left to air-dry for 30min. Subsequently biofilm biomass was stained with 200 µL 0.2% (w/v) of a crystal violet solution, added to each well, and incubated for 15 min at room temperature. Excess stain was then removed and wells washed three times with PBS, the whole plate was then air dried for 30min. Lastly, to solubilize bound dye 200 µL 30% (v/v) acetic acid were pipetted in each well, and left to incubate at room temperature for 15 min with gentle shaking, 200 µL of the solubilized dye was transferred to a fresh plate and absorbance read at 570 nm and 595 nm to quantify biofilm biomass.

RESULTS

Microorganism Isolation and Initial Colour Screening

Following the plating of environmental samples as described in the material and method section, an initial screening of colour was performed, in this case single colonies that displayed pigmentations were picked from mixed culture plates, to be further propagated, until a pure culture was obtained. If an axenic culture was produced and the colonies maintained a pigmented phenotype, the selected organism was inoculated in liquid media, to produce a glycerol stock.

Taxonomic identification of pigmented microorganisms

A Marker Gene approach was adopted to identify isolated microorganisms, based on the sequencing of universal phylogenetic markers such as the 16S rRNA gene for bacteria and ITS sequences for yeasts, as these sequences contain both highly conserved regions ideal for designing universal PCR primers and hypervariable internal regions that are species-specific (e.g., V3, V4, ITS1, ITS2), allowing for the identification of microbial species.

Thus, 59 pigmented strains were identified as reported in table 1: 1 strain isolated from sediments on the hull of a boat in Rimini, 1 strain from fallen foliage in Valpiana, 2 strains isolated from snow on the Presena glacier, 15 strains from marine sediments in Vulcano (including 8 from the sulphur vent area, 5 from samples collected near algal populations, and 2 isolated from samples with bacterial biofilms), 4 strains from cryoconite samples (1 from Italy and 3 from Iceland), and finally from the sampling campaign carried out in Panarea, 8 strains were isolated from *Posidonia oceanica*, 7 from pink *Caryophyllia inornata*, 6 from white *Caryophyllia inornata*, 2 from *Astroides calycularis*, and 13 strains from *Balanophyllia europaea*. No pigmented microorganisms were isolated from samples of *Leptosammia pruvoti* or brown *Caryophyllia inornata*.

Identified strains				
Source	Growth media	Organism name	Strain ID	Color
Boat hull	Vogel	Oxalobacter sp.	MT3	Yellow
Fallen leaves on alpine snow, 1500 m	Vogel	Rhodosporidiobolus colostri (strain 1)	MT4	Pink
Alpine snow, 3000 m	Vogel	Pseudomonas sp.	MT5	Yellow
Alpine snow, 3000 m	Vogel	Rhodosporidiobolus colostri (strain 2)	MT6	Pink
Marine sediment, sulphuric	Marine	Cytobacillus dafuensis	MT7	Yellow
Marine sediment, sulphuric	Marine	Alkalihalobacillus algicola	MT8	Orange
Marine sediment, sulphuric	Marine	Niallia circulans	MT9	Yellow
Marine sediment, sulphuric	Marine	Alkalihalophilus pseudofirmus	MT10	Yellow
Marine sediment, sulphuric	Marine	Sporosarcina luteol	MT11	Yellow
Marine sediment, vegetated	TSA	Psychrobacter alimentarius	MT12	Yellow
Marine sediment, sulphuric	TSA	Neobacillus bataviensis	MT13	Yellow
Marine sediment, microbial mat	TSA	Cytobacillus oceanisediminis	MT14	Orange/Red
Marine sediment, microbial mat	TSA	Bacillus timonensis	MT15	Yellow
Marine sediment, sulphuric	TSA	Micrococcus yunnanensis	MT16	Greenish yellow
Marine sediment, microbial mat	TSA	Bacillus aerius	MT17	Yellow
Marine sediment, sulphuric	TSA	Brevibacillus halotolerans (Strain 1)	MT18	Amber
Marine sediment, microbial mat	TSA	Rossellomorea aquimaris	MT19	Orange
Marine sediment, microbial mat	TSA	Brevibacillus halotolerans (Strain 2)	MT20	Orange
Marine sediment, vegetated	TSA	Aureobasidium namibiae	MT21	Yellow to orange
Italian cryoconite	TSA	Pseudomonas fluorescens group	MT22	Cream Yellow
Iceland cryoconite	TSA	Pseudomonas marginalis	MT23	Red & Yellow (changing)
Iceland cryoconite	TSA	Pseudomonas germanica	MT24	Cream Yellow
Iceland cryoconite	TSA	Pseudomonas arenae	MT25	Red & Yellow (changing)
P. oceanica	Marine	Paracoccus marcusii	MT26	Orange
C. Inornata (White)	CN	Cladosporium sp.	MT27	Reddish
P. oceanica	Marine	Microbacterium paraoxydans	MT28	Light orange
P. oceanica	TSA	Kocuria palustris	MT29	Yellow
P. oceanica	CN	Aureimonas altamirensis	MT30	Yellow
P. oceanica	CN	Myrmecridium normannianum	MT31	Light orange
P. oceanica	TSA	Staphylococcus warneri	MT32	Yellow
C. Inornata (Pink)	TSA	Pseudoalteromonas lipolytica	MT33	Amber
C. Inornata (Pink)	CN	Cobetia amphilecti	MT34	Yellow
B. Europaea	Marine	Shewanella japonica (strain 1)	MT35	Amber orange
C. Inornata (Pink)	CN	Metabacillus idriensis	MT36	Amber yellow
C. Inornata (Pink)	Marine	Planococcus glaciei (strain 1)	MT37	Amber orange
C. Inornata (White)	CN	Planococcus glaciei (strain 2)	MT38	Yellow
A. Calyculares	Marine	Vibrio gigantis	MT39	Light amber
A. Calyculares	Marine	Vibrio sp.	MT40	Light amber
C. Inornata (White)	CN	Cladosporium sp. (strain 1)	MT41	Black
C. Inornata (Pink)	CN	Cladosporium sp. (strain 2)	MT42	Black
C. Inornata (Pink)	CN	Cladosporium sp. (strain 3)	MT43	Black
C. Inornata (White)	CN	Cladosporium aggregatocicaticatum (strain 1)	MT44	Black
C. Inornata (White)	CN	Cladosporium aggregatocicaticatum (strain 2)	MT45	Black
C. Inornata (White)	CN	Cladosporium aggregatocicaticatum (strain 3)	MT46	Black
P. oceanica	Marine	Shewanella japonica (strain 2)	MT47	Amber orange
P. oceanica	CN	Leohumicola minima	MT48	Light pink
C. Inornata (White)	TSA	Alternaria sp.	MT50	Light pink
B. Europaea	CN	Vreelandella piezotolerans	MT51	Amber orange
B. Europaea	CN	Vreelandella sulfidaeris Esulfide	MT52	Amber orange
B. Europaea	CN	Qipengyuania flava (strain 1)	MT53	Yellow
B. Europaea	CN	Qipengyuania qiaonensis (strain 1)	MT54	Yellow
B. Europaea	CN	Qipengyuania qiaonensis (strain 2)	MT55	Yellow
B. Europaea	CN	Bacillus weihaiensis	MT56	Light pink
B. Europaea	CN	Vreelandella aquamarina	MT57	Light pink
B. Europaea	CZ	Psychrobacter pacificensis	MT58	Light pink
B. Europaea	CN	Bacillus weihaiensis	MT59	Yellow
B. Europaea	CN	Qipengyuania qiaonensis (strain 3)	MT60	Yellow
B. Europaea	CN	Qipengyuania flava (strain 2)	MT61	Yellow
B. Europaea	CN	Qipengyuania qiaonensis (strain 4)	MT62	Yellow

Table 1: Table reporting all Isolated and identified strains

Absorbance values at 600 nm

To estimate microbial biomass in suspension during the stationary growth phase, the absorbance at 600 nm was measured for all isolated microbial strains. In the table below (table 2) measured absorbance values, dilution factor and corrected absorbance values are reported for all strains. A higher dilution factor and higher Corrected

Absorbance, indicate an overall higher cell density, which can be a desirable property for the industrial applicability of the strains.

Identified strains					
Organism name	Strain ID	Color	ABS 600 nm	Dilution	ABSCorrected 600 nm
Oxalobacter sp.	MT3	Yellow	0.185	10	1.85
Rhodosporidiobolus colostri (strain 1)	MT4	Pink	0.889	10	8.89
Pseudomonas sp.	MT5	Yellow	0.624	10	6.24
Rhodosporidiobolus colostri (strain 2)	MT6	Pink	0.624	10	6.24
Cytobacillus dafuensis	MT7	Yellow	0.090	10	0.90
Alkalihalobacillus algicola	MT8	Orange	0.131	10	1.31
Niallia circulans	MT9	Yellow	0.040	10	0.40
Alkalihalophilus pseudofirmus	MT10	Yellow	0.070	10	0.70
Sporosarcina luteol	MT11	Yellow	0.172	10	1.72
Psychrobacter alimentarius	MT12	Yellow	0.146	100	14.60
Neobacillus bataviensis	MT13	Yellow	0.103	10	1.03
Cytobacillus oceanisediminis	MT14	Orange/Red	0.117	10	1.17
Bacillus timonensis	MT15	Yellow	0.070	10	0.70
Micrococcus yunnanensis	MT16	Greenish yellow	0.244	100	24.40
Bacillus aerius	MT17	Yellow	0.290	10	2.90
Brevibacillus halotolerans (Strain 1)	MT18	Amber	0.243	10	2.43
Rossellomorea aquimaris	MT19	Orange	0.315	10	3.15
Brevibacillus halotolerans (Strain 2)	MT20	Orange	0.223	10	2.23
Aureobasidium namibiae	MT21	Yellow to orange	0.662	10	6.62
Pseudomonas fluorescens group	MT22	Cream Yellow	0.503	10	5.03
Pseudomonas marginalis	MT23	Red & Yellow (changing)	0.077	10	0.77
Pseudomonas germanica	MT24	Cream Yellow	0.493	10	4.93
Pseudomonas arenae	MT25	Red & Yellow (changing)	0.442	10	4.42
Paracoccus marcusii	MT26	Orange	0.431	10	4.31
Cladosporium sp.	MT27	Reddish	0.025	10	0.25
Microbacterium paraoxydans	MT28	Light orange	0.821	10	8.21
Kocuria palustris	MT29	Yellow	0.336	100	33.60
Aureimonas altamirensis	MT30	Yellow	0.600	10	6.00
Myrmecridium normannianum	MT31	Light orange	0.010	10	0.10
Staphylococcus warneri	MT32	Yellow	0.553	10	5.53
Pseudoalteromonas lipolytica	MT33	Amber	0.170	10	1.70
Shewanella japonica (strain 1)	MT35	Amber orange	0.239	10	2.39
Metabacillus idriensis	MT36	Amber yellow	0.057	10	0.57
Planococcus glaciei (strain 1)	MT37	Amber orange	0.150	100	15.00
Planococcus glaciei (strain 2)	MT38	Yellow	0.140	100	14.00
Vibrio gigantis	MT39	Light amber	0.061	10	0.61
Vibrio sp.	MT40	Light amber	0.128	10	1.28
Cladosporium sp. (strain 1)	MT41	Black	0.042	2	0.08
Cladosporium sp. (strain 2)	MT42	Black	0.014	10	0.14
Cladosporium aggregatocicaticatum (strain 1)	MT44	Black	0.020	10	0.20
Cladosporium aggregatocicaticatum (strain 2)	MT45	Black	0.033	10	0.33
Cladosporium aggregatocicaticatum (strain 3)	MT46	Black	0.013	10	0.13
Shewanella japonica (strain 2)	MT47	Amber orange	0.181	10	1.81
Leohumicola minima	MT48	Light pink	0.009	10	0.09
Alternaria sp.	MT50	Light pink	0.014	10	0.14
Vreelandella piezotolerans	MT51	Amber orange	0.326	10	3.26
Vreelandella sulfidaeris E sulfide	MT52	Amber orange	0.364	10	3.64
Qipengyuania flava (strain 1)	MT53	Yellow	0.056	10	0.56
Qipengyuania qiaonensis (strain 1)	MT54	Yellow	0.011	10	0.11
Qipengyuania qiaonensis (strain 2)	MT55	Yellow	0.253	10	2.53
Bacillus weihaiensis	MT56	Light pink	0.204	10	2.04
Vreelandella aquamarina	MT57	Light pink	0.456	10	4.56
Psychrobacter pacificensis	MT58	Light pink	0.380	10	3.80
Qipengyuania qiaonensis (strain 3)	MT60	Yellow	0.303	10	3.03
Qipengyuania flava (strain 2)	MT61	Yellow	0.197	10	1.97
Qipengyuania qiaonensis (strain 4)	MT62	Yellow	0.065	10	0.65

Table 2: Table showing absorbance values for isolated strains

Evaluation and cataloguing of pigmentation in isolated strains

To compare the pigmentation of the isolated strains, photographs were taken of both the liquid cultures at the end of the stationary phase and the cellular pellets obtained after centrifugation. The images were then assembled into a panel, associating each strain with its specific growth conditions, in order to facilitate a direct comparison of chromatic variations.

Many organisms showed intense coloration, in shades compatible with colour tones of natural anthraquinones, such as the pink observed in both the liquid culture and the cellular pellet of *Rhodosporidiobolus colostri (strain2)*, the bright orange produced by *Paracoccus marcusii*, *Planococcus glaciei (from CIR)*, and *Microbacterium paraoxydans* or yellow of *Micrococcus yunnanensis (RAZ24)* and several shades of brown, such as those produced by *Alkalihalobacillus algicola (RAZ4)*, *Cytobacillus oceanisediminis (RAM20).*

Among the isolated organisms 3 strains of *Pseudomonas* exhibited the ability to release pigments in the culture broth, *Pseudomonas fluorescens, Pseudomonas germanica* and *Pseudomonas arenae*, the same can be said for one strain of *Paracoccus*, *Paracoccus marcusii* and for 6 strains of *Cladosporium*.

Selection of candidate strains to further characterize

Based on the evaluation of pigmentation, which enabled the identification of strains with promising tones for anthraquinone pigment production, and on absorbance data at 600 nm—used to quantify the cellular growth of the various microbial strains—seven microorganisms were selected: *Rhodosporidiobolus colostri*, *Alkalihalobacillus* algicola, *Bacillus oceanisediminis*, *Micrococcus yunnanensis*, *Paracoccus marcusii*, *Planococcus glaciei*, and *Cladosporium aggregatocicatricatum*. The selection was based on a combination of chromatic performance and the ability to reach high cell densities, taking into account the use of cost-effective and readily available culture substrates, with a view toward industrial applicability.

Characterization of selected strains, Growth Curves

Cell growth was evaluated by measuring light absorbance of the culture media at 600 nm at regular two-hour intervals. Subsequently, absorbance data and time measurements were fitted to the logistic equation (Equation 2) using the R software environment. Through dedicated R packages, growth curves were visualized for each organism, and the specific growth rate (r)—the maximum growth speed achievable

under the selected conditions—was calculated, expressed as the expected increase per unit of time (h^{-1}). Additionally, the carrying capacity (K) of the system was estimated, representing the maximum population sustainably supported under the chosen conditions. This value was expressed using the same unit of measurement adopted to quantify population growth.

Below are reported the curves obtained for each selected strain of interest, alongside with the calculated kinetic parameters describing the curve and duplication time:

Rhodosporidiobolus colostri

Organism	K	R	Duplication time	Terrain
Rhodosporidiobolus colostri	7.28	0.35	1H 59min	TSB

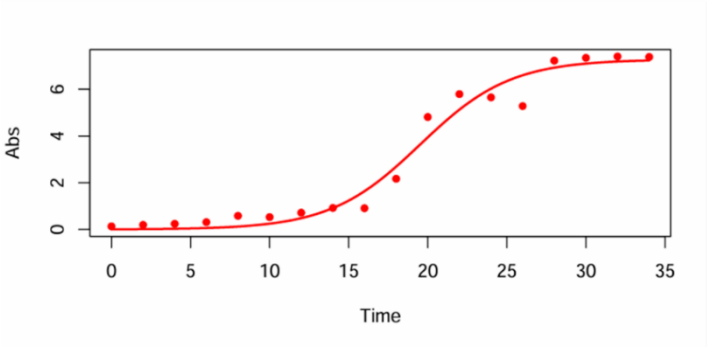

Figure 1: Plotted curve and calculated growth parameters for R. colostri

The curve for R. colostri was obtained after monitoring its growth for 34 hours, in TSB at 20 °C, specific growth rate (r) was 0.35 h^{-1}, carrying capacity (K) of the system was 7.28 Abs and duplication time was calculated to be 1 hour and 59 minutes.

Cytobacillus oceanosediminis

Organism	K	R	Duplication time	Terrain
Cytobacillus oceanosediminis	3.87	0.39	1H 47min	TSB

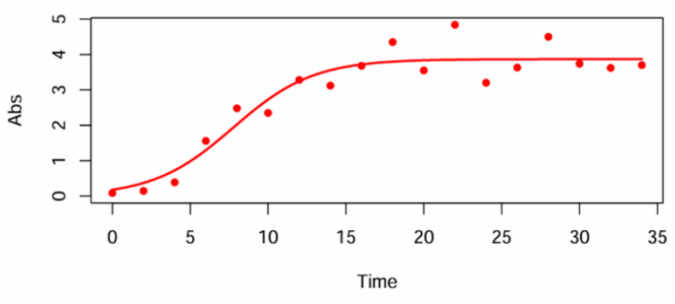

Figure 2: Plotted curve and calculated growth parameters for C. oceanosediminis

The curve for *C. oceanosediminis* was obtained after monitoring its growth for 34 hours, in TSB at 30 °C, specific growth rate (r) was 0.39 h^{-1}, carrying capacity (K) of the system was 3.87 Abs and duplication time was calculated to be 1 hour and 47 minutes.

Micrococcus yuannensis

Organism	K	R	Duplication time	Terrain
Micrococcus yuannensis	19.7	0.3	2H 17min	TSB

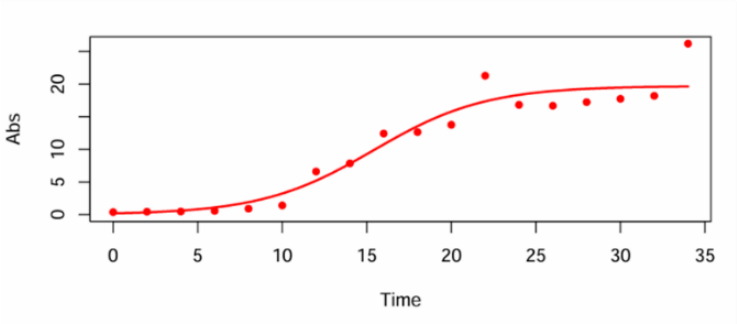

Figure 3: Plotted curve and calculated growth parameters for M. yunnannensis

The curve for *M. yunnannensis* was obtained after monitoring its growth for 34 hours, in TSB at 30 °C, specific growth rate (r) was 0.3 h^{-1}, carrying capacity (K) of the system was 19.7 Abs and duplication time was calculated to be 2 hour and 17 minutes.

Alkalihalobacillus algicola

Organism	K	R	Duplication time	Terrain
Alkalihalobacillus algicola	7.28	0.28	2H 31min	Marine broth

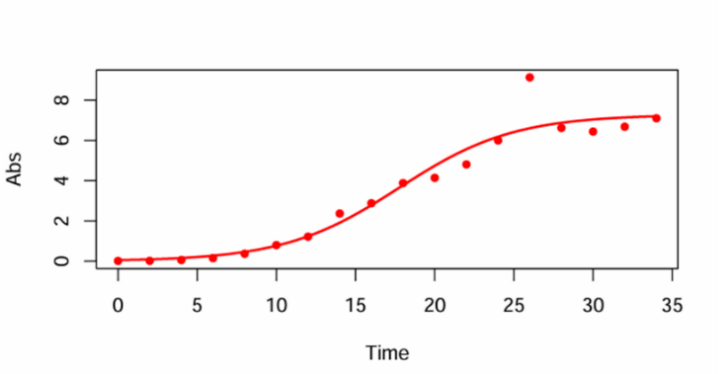

Figure 4: Plotted curve and calculated growth parameters for A. algicola

The curve for *A. algicola* was obtained after monitoring its growth for 34 hours, in TSB at 30 °C, specific growth rate (r) was 0.28 h^{-1}, carrying capacity (K) of the system was 7.28 Abs and duplication time was calculated to be 2 hour and 31 minutes.

Paracoccus marcusii

Organism	K	R	Duplication time	Terrain
Paracoccus marcusii	6.75	0.37	1H 53min	Marine broth

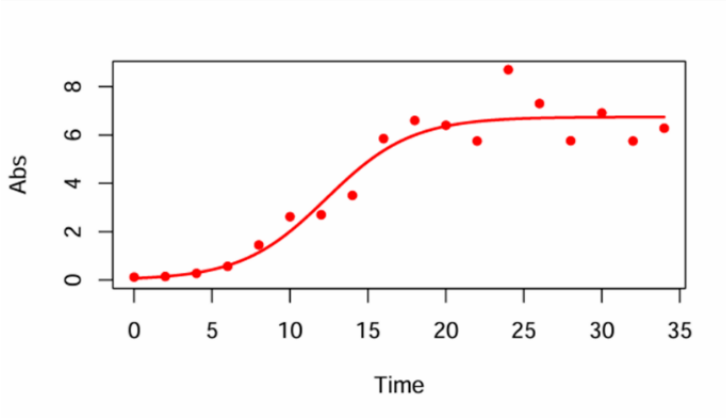

Figure 5: Plotted curve and calculated growth parameters for P. marcusii

The curve for *P. marcusii* was obtained after monitoring its growth for 34 hours, in TSB at 25 °C, specific growth rate (r) was 0.37 h^{-1}, carrying capacity (K) of the system was 6.75 Abs and duplication time was calculated to be 1 hour and 53 minutes.

Planococcus glaciei

Organism	K	R	Duplication time	Terrain
Planococcus glaciei	8.67	0.31	2H 16min	Marine broth

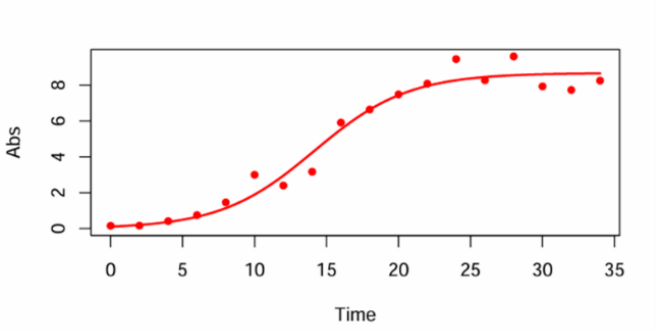

Figure 6: Plotted curve and calculated growth parameters for P. glacei

The curve for *P. glacei* was obtained after monitoring its growth for 34 hours, in TSB at 25 °C, specific growth rate (r) was 0.31 h^{-1}, carrying capacity (K) of the system was 8.67 Abs and duplication time was calculated to be 2 hour and 16 minutes.

Characterization of selected strains, Carbohydrate's metabolism

Inoculated API 50 CH kits (Figure 7) were monitored over the course of two days after 24 and 48 hours, as per producer's instructions, and each change of colour in the media was recorded.

Figure 7: example of an API 50 CH Kit after inoculation of C. oceanosediminis and incubation for 48, absence of growth is marked by red colour in a cupule (Reference cupule 0) gradual coloration toward orange marks the presence of metabolic activity and microbial growth, presence of yellow marks a higher degree of metabolic activity and microbial growth. Cupule 25 turns a different colour (Black) when in presence of metabolic activity compared the other cupules, but remains red in absence of microbial growth.

Results from the 48 hours incubation of API kits were than recorded and compiled in the following table.

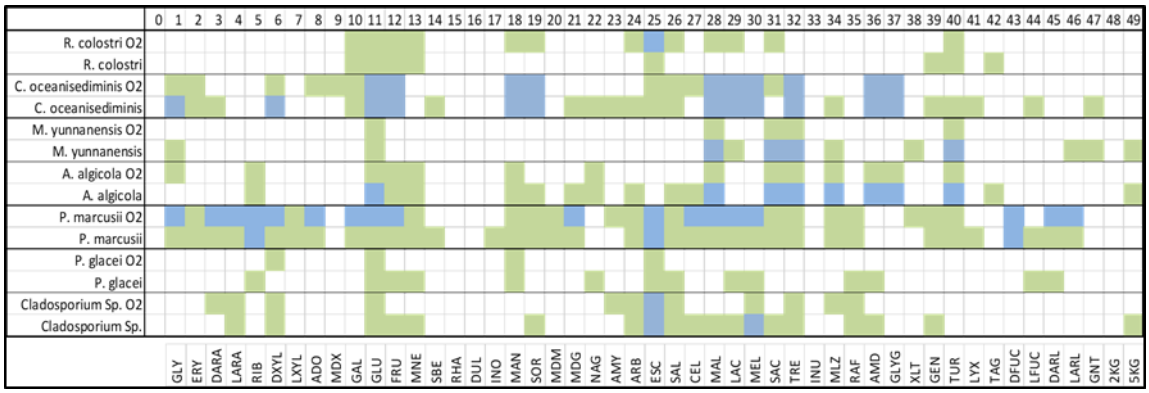

Table 3: This table summarizes the results obtained for each of the strains tested, both under aerobic (Marked by O2) and anaerobic conditions, green squares indicate presence of metabolic activity, blue squares indicate presence of more intense metabolic activity. Numbers in the upper row refer to the number of each cupule, while acronyms in the lower row refer to the compound found inside each cupule.

In general, all seven strains were able to grow within the API 50 CH strips, in both aerobic and anaerobic conditions, although with different modalities and substrate preferences. The only substrate metabolized by all was strains was glucose (GLU, Cupule 11)

R. colostri showed the ability to grow on 13 substrates during aerobic growth and on 8 substrates during anaerobic incubation, Esculin Ferric citrate (ESC, Cupule 25) was the the only substrate that induced higher metabolic activity, if incubated in the presence of oxygen.

C. oceanosediminis showed the ability to grow on 20 substrates in the presence of oxygen and on 28 substrates in the absence of oxygen, *C. oceanosediminis* showed signals of higher metabolic activity while growing on 12 substrates (GLY, Cupule 1. DXYL, Cupule 6. GLU, Cupule 11. FRU, Cupule12. MAN, Cupule18. SOR, Cupule 19. MAL, Cupule 28. LAC, Cupule 29. MEL, Cupule 30. TRE, Cupule 32. AMD, Cupule 36. GLYG, Cupule 37.), of those, Glycerol (GLY) and D-Xylose (DXYL) only resulted in higher metabolic activity during growth without oxygen, while for the remaining compounds all showed signals of higher metabolic activity by *C. oceanosediminis* when it grew both in aerobic and anaerobic conditions.

M. yunnannensis was able to grow on 5 substrates while cultivated in the presence of oxygen and showed signs of metabolic activity on 12 substrates while growing in anaerobic conditions, *M. yunnannensis* showed higher metabolic activity while growing on four substrates (CEL, Cupule 28. SAC, Cupule 31. TRE, Cupule 32. TUR Cupule 40) interestingly though, only when grown in anaerobic conditions.

A. algicola showed the ability to grow on 14 substrates while incubated in the presence of oxygen, and the ability to grow on 20 substrates while incubated under anaerobic conditions, on 8 of which it showed a higher metabolic activity (GLU, Cupule 11. CEL,

Cupule 28. SAC, Cupule 31. TRE, Cupule 32. MLZ, Cupule 34. AMD, Cupule 36. GLYG, Cupule 37. TUR Cupule 40)

P. marcusii showed extended metabolic capabilities, being able to grow on most of the substrates present in the strips, in particular; on 34 substrates while growing in aerobic conditions and on 36 substrates while growing in the absence of oxygen. It also showed the induction of higher metabolic activity while growing on 18 different substrates in aerobiosis (GLY, Cupule 1. DARA, Cupule 3. LARA, Cupule 4. RIB, Cupule 5. DYXL, Cupule 6. ADO, Cupule 8. GAL, Cupule 10. GLU, Cupule 11. FRU, Cupule 12. MDG, Cupule 21. ESC, Cupule 25. CEL, Cupule 27. MAL, Cupule 28. LAC, Cupule 29. MEL, Cupule 30. DFUC, Cupule 43. DARL, Cupule 45. LARL, Cupule 46). The number was reduced to three if considering anaerobic conditions (RIB, Cupule 5. ESC, Cupule 25. DFUC, Cupule 43).

P. glacei presented the ability to grow on 4 different substrates while incubated in the presence of oxygen and showed signs of metabolic activity on 14 substrates while incubated inanaerobic conditions. Under no conditions *P. glacei* showed signs of higher metabolic activity.

Cladosporium sp. showed the ability to grow inside 12 cupules while incubated in aerobiosis and the ability to grow inside 19 cupules while incubated in anaerobiosis. Moreover, it showed signals of higher metabolic activity 2 on two substrates when incubated in the absence of oxygen (ESC, Cupule 25. MEL, Cupule 30), while when incubated in the presence of oxygen only one substrate gave rise to higher signals of metabolic activity (ESC, Cupule 25).

Finally, of the selected organisms none was able to grow on these four substrates: L-Rhamnose (RHA, Cupule 15), Dulcitol (DUL, Cupule 16), Inulin (INU, Cupule 33) and Potassium 2-ketogluconate (2KG, Cupule 48).

Characterization of selected strains, Genome sequencing, Phylogeny reconstruction and BGCs Prediction

After the genomes of selected strains had been successfully sequenced, obtained reads were assembled into contigs and finally into complete genome assemblies. Each of these assemblies were then characterized in terms of length, completeness and coverage while their quality was assessed using standard quality metric such as N50, L50 and length of the largest contig. Subsequently a genome mining analysis was performed to identify BGCs present in the assemblies, when one biosynthetic gene cluster was identified, it was assigned a type and a putative product based on similarity with known BGCs.

Regarding the first strain, *R. colostri* genome was estimated to be 24,411,120 bp in length, with a completeness of 98% and a sequencing depth of 56x, GC content measured to be 59,90%. The largest contig yielded by the assembly was 277,999 bp long, N50 was calculated to be 43,781 bp, with an L50 of 156 contigs. Genome mining revealed the presence of 5 BGCs, three were assigned to the family of terpene producing BGCs while the remaining two where categorized NRPS-like. Of the three Terpene type clusters, one was putatively assigned ascofuranone as the final product, one was assigned a general carotenoid as final product of biosynthesis and to the last one a putative assignment of product couldn't be achieved.

Cytobacillus oceanosediminis genome was estimated to be 4,895,040 bp, completeness was 87% while sequencing depth obtained was 153x, with a 46,01% GC content. Largest conting was 70,829 bp, N50 was calculated to be 515,084 bp and a L50 of 4 contigs. Relative to the biosynthetic capabilities of this microorganism, its genome revealed the presence of 5 BGCs, three were classified as belonging to the terpene family, one to type-three polyketide synthase family and the last one to the Class-II lanthipeptide family. Among the terpene clusters, one was putatively assigned to alkylresorcinol biosynthesis, one to carotenoid biosynthesis and the third couldn't be assigned to a specific product. As for the Polyketide type BGC it was assigned to fumihopaside A biosynthesis.

Our strain of *Mycrococcus Yunnannensis* genome was estimated to be 2,463,766 pb, its completeness percentage was 96%, with a GC content reaching 73.12% and depth of sequencing reached a 328x coverage. Largest contig obtained was 362,215 bp long, with a N50 contig 268,519 bp long and a calculated L50 of 4 contigs. Mining this genome assembly for the presence of BGCs revealed 6, they were all assigned to different families, in particular: one was assigned to ectoine producing family, one to RRE-containing BGCs, one to the beta lactone producing family, one to terpene producing family, one to NAPAA class of BGCs and the last one to Ni-siderophore producing family. Of these the BGC pertaining to the terpene producing family has been associated to the production of a carotenoid like molecule.

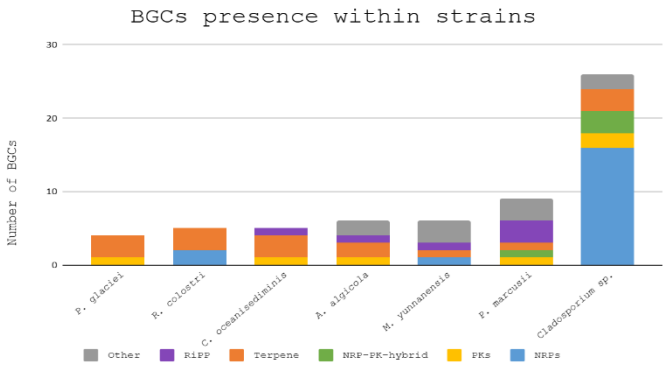

Figure 1: Distribution of BGCs types within the genomes of selected strains, types are based on antiSMASH categorization.

The genome of *Alkhalihalobacillus algicola*, was estimated to measure 4,165,959 bp, its completeness reached 100% when compared against a reference sequence and its coverage reached 154x of sequencing depths, lastly GC content amounted to 40,58%. The longest contig measured 308,061 bp, N50 contig measured 187,244 bp and L50 was 9 contigs. The genome of A. algicola revealed the presence of 6 biosynthetic gene clusters, two pertaining to the terpene producing family, one to the betalactone producing family, one associated with production of Ni containing siderophores, one was categorized as an RRE-containing BGCs and finally the last one was categorized as type three polyketide synthase BGC. Of these, one terpene producing BGC was assigned to the putative production of fumihopaside a, the other terpene producing BGC was assigned to the production of a carotenoid type molecule, while the T3PKS BGC was associate to the putative production of alkyloresorcinol.

The genome of *Paracoccus marcusii* was estimated to measure 4,220,925 bp, its completeness reached 100% when compared against a reference sequence, GC content was measured to be 66,10% and the sequencing coverage was calculated at 158-fold depth of sequencing. The longest contig measured 1,121,956 bp, the N50 contig size was 265,798 bp, and the L50 value was 4 contigs. Analysis of the genome revealed the presence of nine biosynthetic gene clusters. Among these, one terpene cluster was assigned to the putative biosynthesis of a carotenoid pigment, while the type-3 polyketide synthase cluster was associated with alkylresorcinol production, lastly the mixed NRPS–PKS cluster was associated to the putative production of an obafluorin-like molecule.

The genome of *Planococcus glacei* was estimated to be 3,938,246 bp long, its completeness reached 95%, GC content amounted to 46,78% and its depth of sequencing reached a 255-fold coverage. The largest contig constructed measured

1,305,237 bp, the length of N50 was 849,506 and the value of L50 was 2 contigs. The genome of *P. glacei* harbored the presence of four biosynthetic gene clusters, one pertaining to the class of Type-3 poliketidesintase BGC, while the remaining 3 were categorized as terpene producing BGC. In particular the polyketide type BGC was associated with the putative production of Alkylresorcinol, while of the three-terpene type BGCs, two were associated with the putative production of a carotenoid type molecule, while the last terpene type BGC has been associated with the putative production of (2R,3S,4S)-5-fluoro-2,3,4-trihydroxypentanoic acid.

The genome of the *Cladosporium* sp. strain we isolated was estimated to be 25,128,860 bp in length, its completness level was estimated to be 49,63% using ChecKM due to the absence of a comparable reference sequence (Parks, Imelfort et al. 2015), GC content was 53.71% while depth of sequencing reached a 45-fold coverage. The longest contig obtained was 208,515 bp long, N50 measured 50,247 while L50 value was 165 contigs. Analysis of the *Cladosporium* sp. genome revealed 26 biosynthetic gene clusters (BGCs). Among these, seven were identified as pertained to potentially pigment-producing classes. These included two Type I polyketide synthase (T1PKS) BGCs, three characterized as terpene-producing BGCs, and two categorized as hybrid NRPS-T1PKS biosynthetic gene clusters.
More in details, the first T1PKS BGC has been associated to the production of a betaenone-like molecule, the second T1PKS BGC was associated to the production of a naphthalene type molecule, due to a similarity score of 0.53 with the 1,3,6,8-tetrahydroxynaphthalene producing clusters compared with antiSMASH.
Regarding hybrid type NRPS-T1PKS clusters, one was assigned to the putative production of a tetralin derived compound, while the second cluster couldn't be assigned to a specific product. Lastly of the three terpene producing clusters one couldn't be assigned to a specific product. The second cluster was associated with the production of a fumihopaside-like compound and finally the third terpene producing cluster was associated to the production of a carotenoid molecule.

For the seven investigated strain the presence of BGCs was mined and when possible, the corresponding BNC predicted. In total five BGCs yielded a prediction through either Ripp-miner or PRISM, one from *C. oceanosedimins* (C.o._BGC5), one from *P. marcusii* (P.m_BGC7.3) and three from *Cladosporium* sp. (C.sp._BGC9.2, C.sp._BGC15.1, C.sp._BGC49).

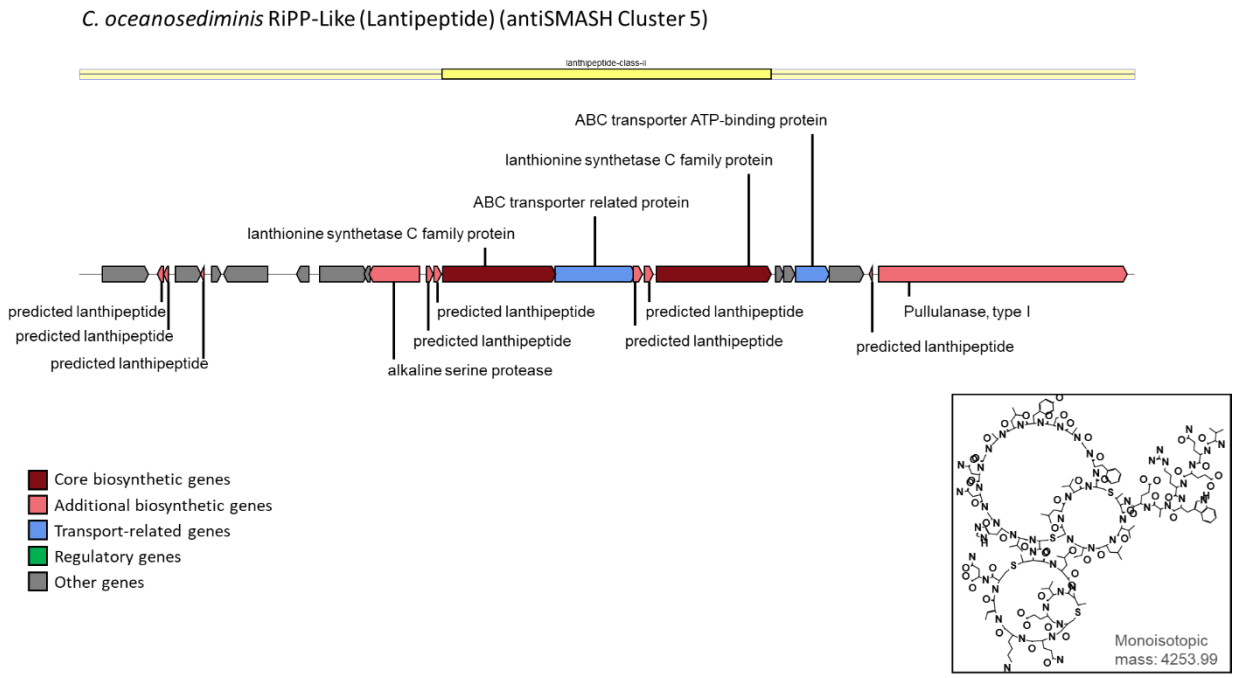

Figure 2: Picture showing sintheny and predicted BNC for a lanthipeptide-class BGC of *C. oceanosediminis*. (C.o._BGC5)

C.o._BGC5 is RiPP-Like cluster of the Lantipeptide class, it consists of two core biosynthetic genes: lanthionine synthtase C proteins and multiple additional biosynthetic genes: eight predicted lanthipeptide sequences, a Pullulanase gene and an alkaline serine protease gene and lastly two transport-related genes coding for ABC transporter proteins.

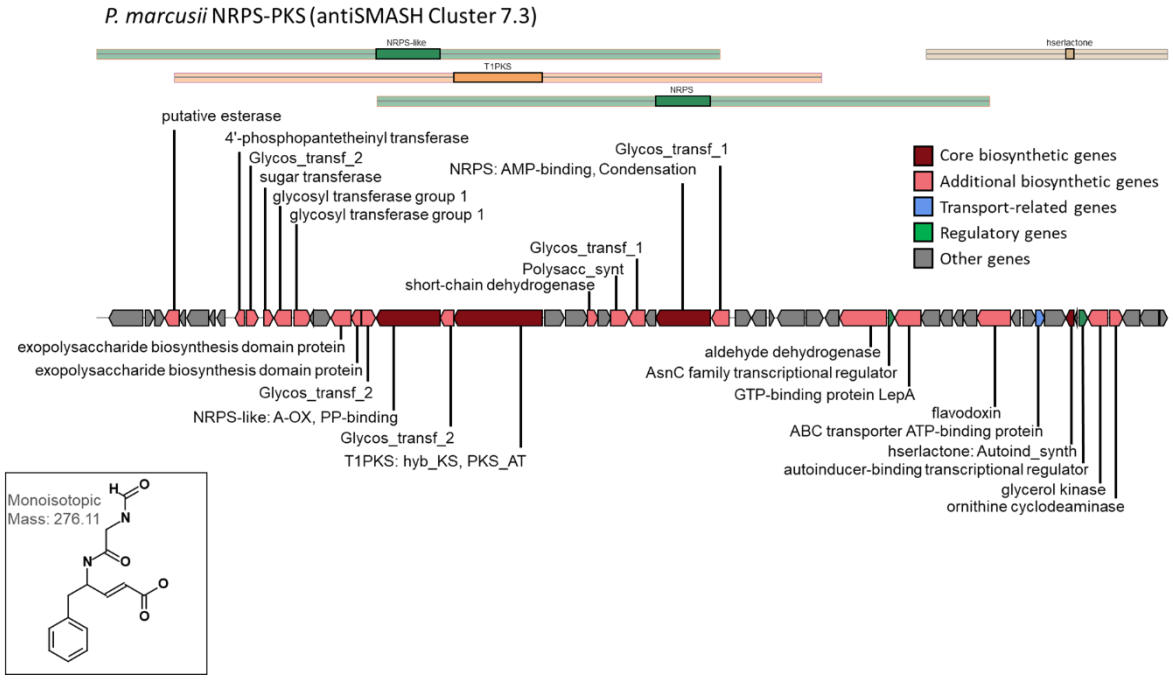

Figure 3: Picture showing the sintheny and predicted BNC for a hybrid NRPS-PKS cluster of *P.marcusii*. (P.m_BGC7.3)

From P.marcusii a hybrid NRPS-PKS cluster (P.m_BGC7.3) was identified, core biosynthetic genes consisted of a Type 1 Poliketide synthase and two NRPS genes, predicted to possess AMP-Binding, Condensation, A-OX and PP-Binding functions. Multiple additional biosynthetic genes are also present, coding for glycosyl transferases and polysaccharide synthesis, this might hint at the inclusion of saccarides moyeties in the final BNC although PRISM did not predict any. To note, P.m_BGC7.3 is bordering another cluster, predicted to be a Homoserine lactone producing BGC, although PRISM did not offer a structural prediction for the cluster product, comparison with other clusters deposited in MiBIG showed it possess an analogous gene organization.

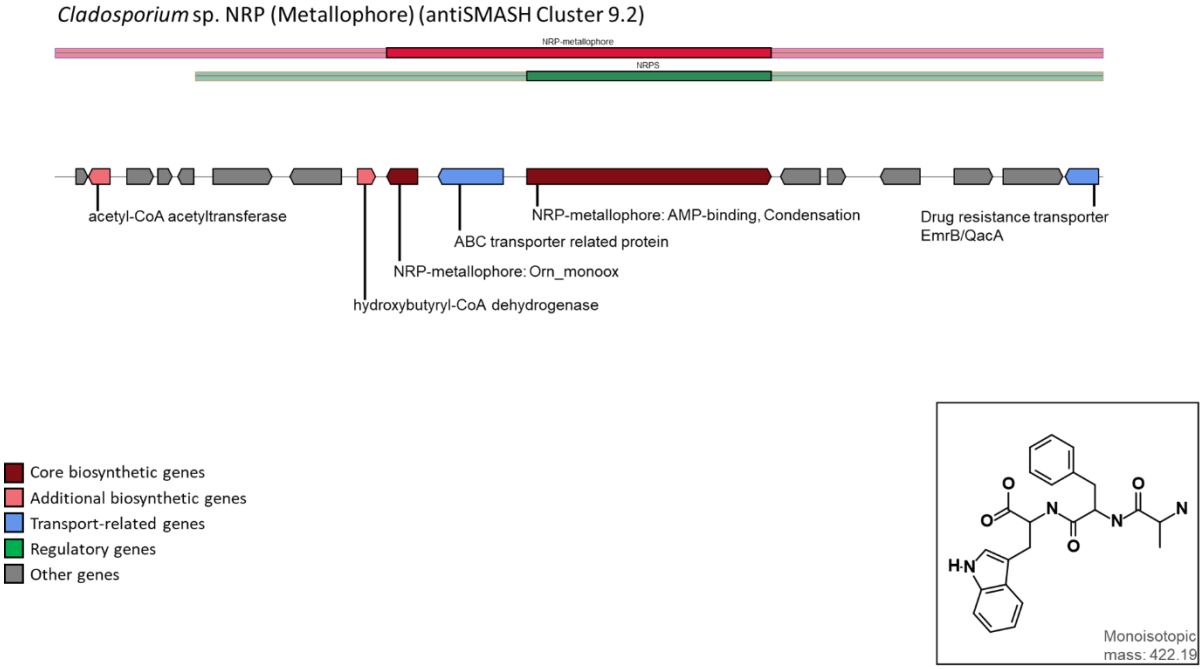

Figure 4: Picture showing the sintheny and predicted BNC for NRPS cluster of *Cladosporium* sp. (C.sp._BGC9.2)

C.sp._BGC9.2 is a NRPS cluster present within *Cladosporium* sp. genome, the core biosynthetic genes have been assigned the NRP-metallophore categorization by antiSMAHS, possesing AMP-binding, Condensation and Ornitine-monooxigenase functions, two additional biosynthetic genes are also present, one coding for acetyl-CoA acetyltransferase and for hydroxybutyryl-CoA dehydrogenase, lastly two genes coding for transport related proteins are also present.

Cladosporium sp. NRPS (antiSMASH Cluster 15.1)

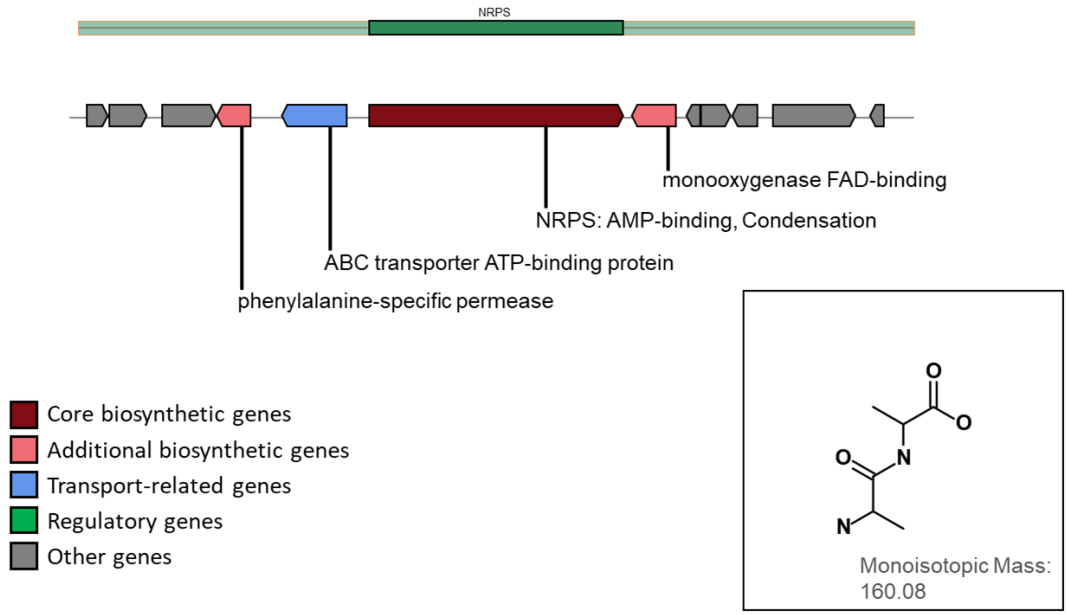

Figure 5: Picture showing the sintheny and predicted BNC for NRPS cluster of *Cladosporium* sp. (C.sp._BGC15.1)

C.sp._BGC15.1 cluster contains one NRPS core biosynthetic gene, with AMP-binding and condensation functions, two additional biosynthetic genes a phenylalanine-specific permease and one gene coding for a monoxygenase FAD-Binding protein, one ABC transporter gene is also present. Although PRISM gave only a di-Ala peptide as structural prediction for the BGC product, a comparison of the core biosynthetic gene with custers deposited in MiBIG, found a sequence identity of 45,34% when aligned against the sequence of cyclo-(D-Phe-L-Phe-D-Val-L-Val) synthetase, from *Penicillium rubens Wisconsi,* indicating that C.sp._BGC15.1 might actually be responsible for the production of a cyclic tetrapeptides containing Alanine.

Cladosporium sp. NRPS (antiSMASH Cluster 49)

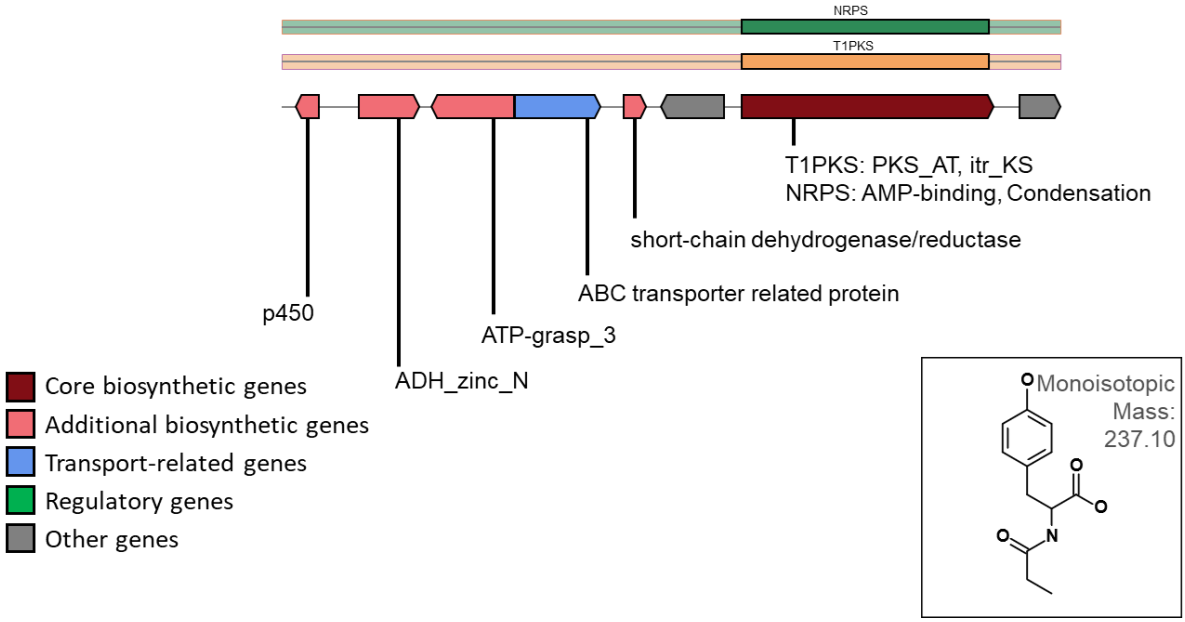

Figure 6: Picture showing the sintheny and predicted BNC for hybrid NRPS-PKS cluster of *Cladosporium* sp. (C.sp._BGC49)

Last cluster yielding a structural prediction from PRISM was C.sp._BGC49, core biosynthetic gene is a hybrid NRPS-PKS predicted to have the following domains: PKS_AT, AMP-binding and Condensation. The cluster present one transport related gene coding for an ABC transporter protein. Four additional biosynthetic genes are present: a Cytochrome p450 gene, an alcohol deidrogenase coding gene (ADH_zinc_N), an ATP-grasp_3 gene and finally a short-chain dehydrogenase/reductase. When compared against MiBIG deposited clusters, it showed anologous gene organization to Varicidin A producing cluster (BGC0002304) from *Talaromyces variabilis* and high percentage identity, over alignment of the two hybrid NRPS-PKS amino acid sequences with 36.56%, the two ATP_grasp3 sequences with 41.57% and the ADH_zinc_N sequences with 34.38%.

Characterization of selected strains, Chemical characterization:

UPLC-MS analysis

As a result of the targeted UPLC-MS analysis three anthraquinone molecules were identified to be present in some of the produced extracts, in particular: extract of P. glacei contained: Physcion 0,018 µg/ml, Carminic acid 0,042 µg/ml. Extract of R. colostri contained: Rhein 0,03 µg/ml, Physcion 0,015 µg/ml, Carminic acid 0,043 µg/ml. Extract of A. algicola contained: Rhein 0,03 µg/ml, Physcion 0,019 µg/ml, Carminic acid 0,042 µg/ml.

Thus, identifying a presence for these molecules in the extracts, albeit at very low concentrations, making the extraction of these compounds from our strains currently not economically feasible, without some form of elicitation during production and growth.

After the identification of anthraquinone compounds, we characterized the extracts using a non-targeted approach, and found signals related to the presence of multiple secondary metabolites, which are in line with previous predictive genomic analysis we did for the identification of biosynthetic gene clusters, unfortunately due to the lack of molecular standards for each of the possible compounds, a confirmation of presence was currently not possible.

Followingly is a list for signals that match possible compounds present in the extracts: Firstly In the UPLC–MS chromatographic analysis of *Paracoccus marcusii* extracts,

several secondary metabolites were detected, early-eluting, signals corresponded to methyl troposulfenin (Da 226.3, Rt 0.52), roseobacticide C (Da 307.4, Rt 0.66), later in the chromatogram, peaks assigned to adonirubin (Da 580.8, Rt 1.05), paracentrone (Da 462.7, Rt 1.23), tryptanthrin (Da 248.24, Rt 2.47), representing more hydrophobic aromatic compounds. roseobacticide H (Da 362.4, Rt 3.50), rhamnolipid R1 (Da 650.8, Rt 6.48), (2R,3S,3'S)-2-hydroxyastaxanthin (Da 612.8, Rt 14.82), adonixanthin 3-glucoside (Da 745.0, Rt 14.56), and adonicanthin (Da 582.9, Rt 17.58), all characteristic of *Paracoccus* carotenoid biosynthesis pathways. The final signal corresponded to n-tridecan-1-ol (Da 398.7, Rt 18.39). For Planococcus glacei extracts, a more restricted set of metabolites was detected, histidyl-proline diketopiperazine (Da 248.28, Rt 0.66), lisinopril R,S,S-diketopiperazine (Da 387.5, Rt 0.81), 5-glucosyl-5,6-dihydro-4,4´-diapolycopenene Rt 1.31 (Da 766.3), a glycosylated apocarotenoid intermediate indicative of carotenoid biosynthesis. rhamnolipid (Da 334.4, Rt 18.7) and decaprenoxanthin (Da 705.1, Rt 19.08), signals were also present at later times in the chromatogram. In the UPLC–MS chromatographic analysis of *Alkalihalobacillus* algicola extracts, several distinct secondary metabolites were detected, chrysophanol (Da 254.24, Rt 0.87), bacillaene (Da 580.8, Rt 0.91), macrolactin H (Da 402.5, Rt 1.14), surfactin A (Da 1007.65, Rt 18.2) and 7-deoxypactamycin (Da 542.6, Rt 18.5). In addition, difficidin (Da 544.7, Rt 19.2) and bacilysin (Da 270.28, Rt 19.32) were detected. In the UPLC–MS chromatographic analysis of Cytobacillus oceanosediminis extracts, the following molecular profile was detected, macrolactin H (Da 544.7, Rt 0.76), (2R,3S,3'S)-2-hydroxyastaxanthin (Da 564.8, Rt 0.79), chrysophanol (Da 254.24, Rt 0.92), bacillaene (Da 580.8, Rt 19.1), echinenone (Da 550.9, Rt 18.5), canthaxanthin (Da 564.8, Rt 19.45). For Rhodosporidiobolus colostri the UPLC-MS analysis of the extracts detected, canthaxanthin (Da 564.8, Rt 16.08), torularhodin (Da 564.8, Rt 16.08), adonirubin (Da 580.8, Rt 17.4) and 2-hydroxytorularhodin (Da 580.8, Rt 17.4). Finally in the UPLC–MS chromatographic analysis of *Cladosporium* sp. extracts, a diverse array of secondary metabolites was detected, isocladosporin and cladosporin (Da292.33, Rt 0.75), endocrocin (Da314.25, Rt 0.77),1,8-dihydroxynaphthalene (Da160.17, Rt 0.82), cladosacid (Da250.33, Rt 0.85), cladospolide (Da228.28, Rt 0.85), cladosporide (Da386.6, Rt 0.92), cladofulvin (Da538.5, Rt 1.61), 2-(4-hydroxy-1,3-dihydro-2-benzofuran-1-yl) acetic acid (Da194.18, Rt 1.6), (±)-3-phenyllactic acid (Da166.17, Rt 2.63), cladosin (Da282.34, Rt 2.32), cladosporol (Da350.3, Rt 2.58), calphostin (Da790.8, Rt 3.29) cladochrome (Da774.8, Rt 2.99), haematocin (Da502.6, Rt 3,16), cladodionen (Da233.26, Rt 3,51), cladosporiumin (Da349.4, Rt 3,99).

Functional characterization of the extracts:

Antioxidant activity

The antioxidant activity of the seven extracts was evaluated using the TAC (Total Antioxidant Capacity) assay, expressed as Trolox equivalents (µM). Among the tested samples, four showed measurable antioxidant activity, while the remaining three did not display significant values.

Specifically, the cellular extracts of *Cladosporium* (82.7 µM) and Rhodosporidiobolus colostri (93.7 µM) exhibited moderate antioxidant capacity. The *Paracoccus marcusii* CFB (1:2) extract showed higher activity (108.8 µM), while the highest value was recorded for the *Cladosporium* CFB extract (211.6 µM).

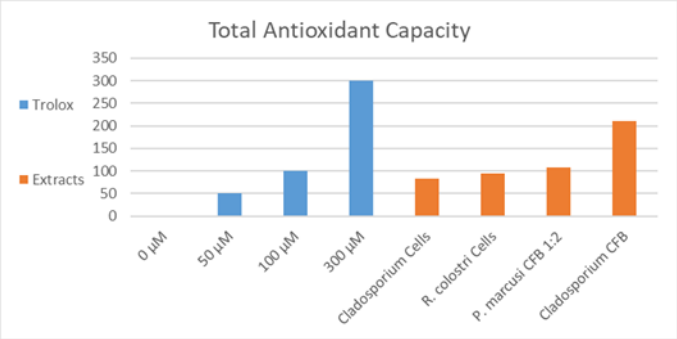

Figure 8: Total Antioxidant Capacity of the extracts expressed as micromolar concentration of Trolox

Overall, these results indicate that the CFB fractions, particularly that of *Cladosporium*, display a markedly higher antioxidant capacity compared to the cellular extracts.

Antimicrobial activity

Firstly, a cross streak antimicrobial assay was performed, to identify which of the seven strains had the ability to produce metabolites with antimicrobial capabilities against 3 reporter organisms: *E. coli*, *P. aeruginosa* and *S. aureus*. This revealed that out of 7 strains *M. yunnannensis* and *P. marcusii* showed signs of antimicrobial activity

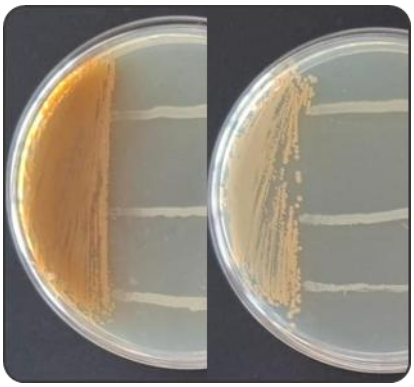

Figure 9: Comparison of two plates from the cross-streak assay: on the left P. marcusii is able to inhibit the growth of reporter strain Escherichia coli CECT416, while on the right P. glacei is not able to inhibit the growth of reporter strain Escherichia coli CECT416

With this information, another assay was performed to measure the reporter strains inhibition, while growing in a liquid culture supplemented with extracts of *M. yunnannensis* and *P. marcusii*

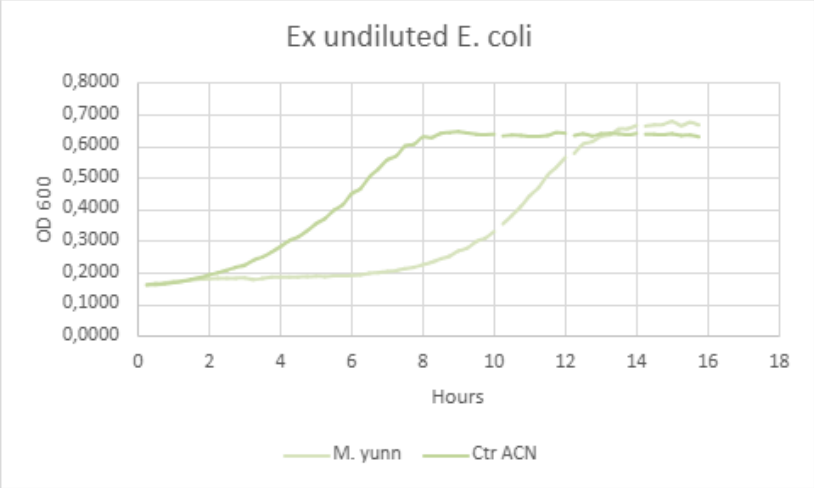

Figure 10: Antimicrobial effect of undiluted extract of M. Yunnannesis over the growth of E. coli, showing a delay in growth.

Regarding the antimicrobial activity of *P. marcusii*, the strain showed good activities against both *E. coli* and *S. aureus* when grown on agar plate, but this only partially translated to the in liquid assay, with extracts produced from *P. marcusii* showing little antimicrobial effect only against *S. aureus* when used undiluted, when a ten times diluted extract was used no inhibition was observed.

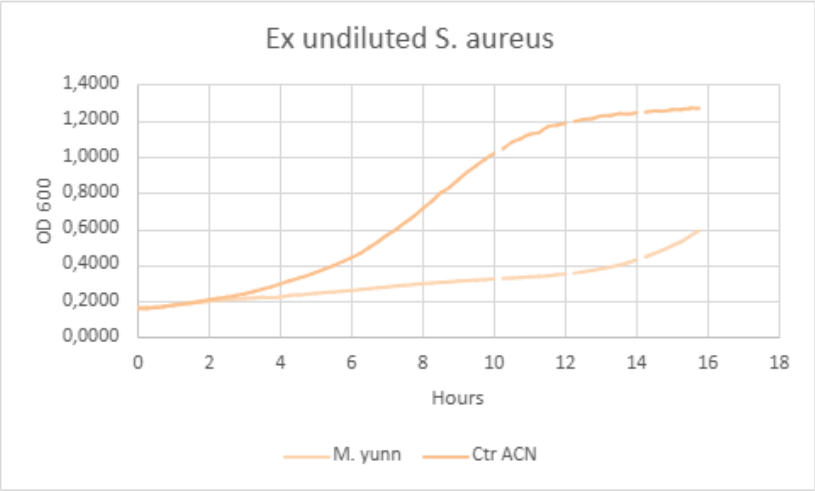

Figure 11: Antimicrobial effect of undiluted extract of M. Yunnannesis over the growth of S. aureus, showing a delay in growth.

Regarding *M. yunnannensis* the extract showed good bacteriostatic properties when employed undiluted against both *E. coli* and *S. aureus*, slowing down growth of both strains by 6 and 8 hours respectively. When employed in a 1/10 dilution, no effect was observed on *E. coli* growth and a minimal action was observed over the growth of *S. aureus*.

Antibiofilm activity

An antibiofilm assay based on crystal violet staining was performed, to assess the effects of four selected extracts on *Pseudomonas aeruginosa* biofilm formation, measuring CV staining as optical density at 570 nm (OD_{570}).

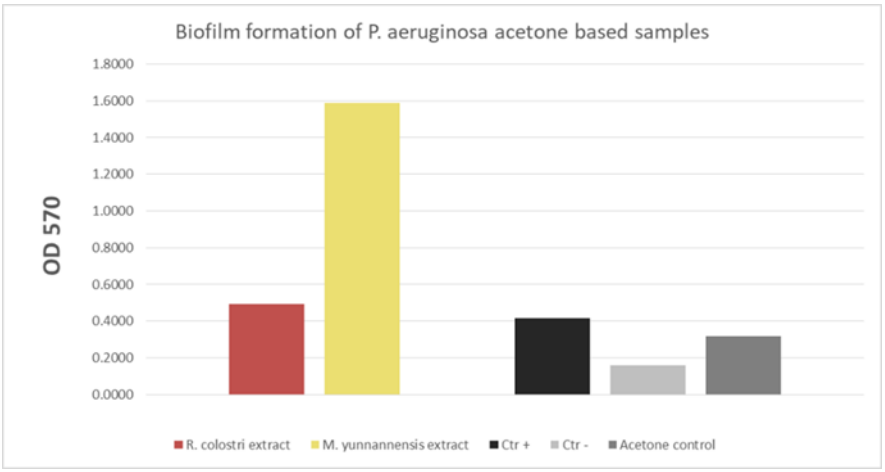

Figure 12: OD values for the biofilm production of P. Aeruginosa treated with Acetone based extracts and controls

When *P. aeruginosa* was treated with acetone-based extracts of *R. colostri* (OD_{570} = 0.4919) it showed a biofilm biomass comparable to the positive control (OD_{570} = 0.4152), whereas when treated with extract from M. yunnannensis (OD_{570} = 1.5872) a higher biofilm formation was promoted. In contrast, the acetone solvent control displayed slightly lower biofilm levels (OD_{570} = 0.3176), while the negative control (OD_{570} = 0.1589) showed the lowest OD value.

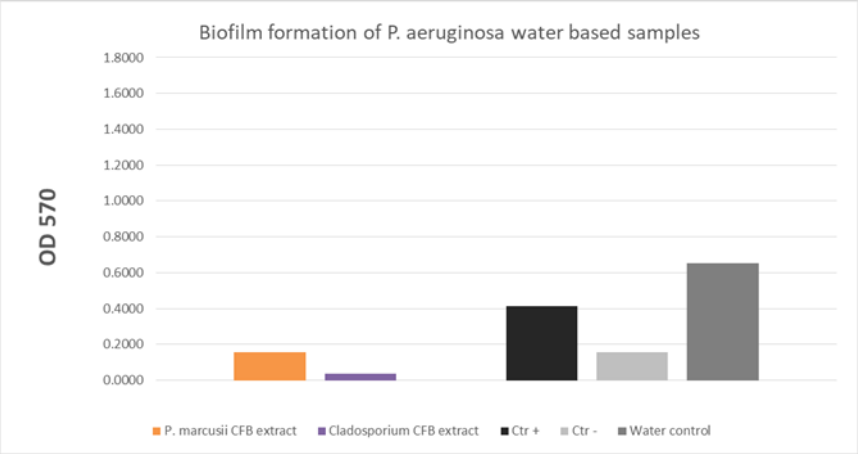

Figure 13: OD values for the biofilm production of P. Aeruginosa treated with Water based extracts and controls

For the treatment with water-based extracts, *P. marcusii* CFB (OD_{570} = 0.1579) and *Cladosporium* CFB (OD_{570} = 0.0391) both exhibited a strong reduction in biofilm formation compared with the positive control (OD_{570} = 0.4152) and the water solvent control (OD_{570} = 0.6539). Suggesting that water based extracts of *Cladosporium* and *P. marcusii* cell free broths exhibited the highest antibiofilm activity.

DISCUSSION

In this work, we set out to explore pigmented microorganisms isolated from diverse, metabolically challenging environments, in order to evaluate their potential as sources of bioactive natural compounds with relevance for textile applications.

UPLC–MS profiling revealed a chemically rich metabolome across the candidate strains. Notably, carotenoid species: canthaxanthin, torularhodin, adonirubin, echinenone, were detected in yeast and bacterial extracts, while a mixture of known fungal secondary metabolites, including anthraquinone-like components such as endocrocin and cladochrome, alongside a broader array of polyketide scaffolds, were observed in

Cladosporium extracts. In addition, signals consistent with several polyketide and macrolide molecules, such as macrolactin H, bacillaene and difficidin were identified in bacterial extracts. These observations indicate that the isolated strains produce both lipophilic pigments, such as carotenoids and polar bioactive polyketides type molecules.

Genome mining confirmed the biosynthetic potential of the selected isolates, with multiple terpenes, NRPS-like and PKS, including a type-III and type-I PKS clusters annotated across genomes for example, R. colostri with terpene and NRPS-like BGCs. Other types of BGCs were also detected such as those related to the production of lanthipeptides and RiPP-compounds as in *C. oceanosediminis* with terpene, PKS-III and lanthipeptide clusters. In general, there was agreement between the genomic and metabolomics data, with the strains possessing the high numbers of predicted BGCs also giving a high number of hits in the chromatographic analysis. however, although UPLC–MS returned signals attributable to anthraquinone-like molecules, direct matches to canonical AQ BGCs were absent in the automated antiSMASH annotation of several genomes. This is likely due to different possible mechanisms: first structural and organizational divergence of AQ biosynthetic loci in non-canonical producers, might reduce similarity to the characterized reference clusters available in databases. Secondly, presence of biosynthetic pathways distributed across multiple, non-contiguous loci or involving trans-acting tailoring enzymes might evade detection by current algorithms; and lastly regulatory activation requirements for specific pathways complicate mapping between genotype and metabolites leading to the identification of unexpressed BGCs.

In this context the results obtained from the strains characterization, regarding their utilization of carbohydrate substrates, could provide some help, in finding better media formulations to induce secondary metabolisms activation, this could especially be attuned to the environment from which the strains were first selected as, they appeared to have similar carbohydrate utilization patterns, as was the case with strains *A. algicola* and *M. yunnannensis*, both of them isolated from volcanic marine sediments, showing a close pattern of utilization especially attuned to malate, or the case with strains *P. glacei* and *Cladosporium* sp. that even though are not closely related with one being a prokaryote and the other an eukaryote, they both show a similar utilization pattern, especially focused on glucose, fructose and mannose, in agreement with being isolated from coral hosts.

CONCLUSION

As previously stated AQs make up a class of molecules with interesting properties that makes them target for use in biotechnological applications and processes such as textile dying or anti-biofilm surface finishing's, that said up until now the production of

anthraquinones in microorganisms was reported only within groups such as *Aspergillus* for fungi and *Actinomyces* for bacteria. These genera have been known for their expansive metabolic and biosynthetic capabilities, but even for some of the most promising strains, direct application in industry without employing strategies such as elicitation or heterologous expression are limited.

In this context, the detection of Anthraquinones inside of microbial species not commonly associated with their production, represents a novelty with possible implications in fields of microbiology and biotechnological. On a first level, reliably finding anthraquinones even in trace amounts, in microbial groups not associated with AQ production indicates that the "research space" has not been fully investigate yet Our approach suggests that a proxy-based isolation pipeline, in which a character such as anthraquinone production cannot be *a priori* selected for, using terrains that favour metabolic plasticity and *a posteriori* selection method, in our case colour which infer the presence of BGCs in microorganism, can be an applicable strategy to select strains of interest that present expanded metabolic capabilities. As a result of the whole genome sequencing and mining for BGCs, all our strains of interest showed the presence of a number of biosynthetic clusters, some classified to be coding for Polyketide synthases and thus possibly associated to Anthraquinone production, though at the end of the genome mining none of the identified BGCs were reported for the specific production of known Anthraquinone or Anthraquinone-like compounds, this is not in concordance with the results obtained from UPLC-MS analysis where signals from Anthraquinones species were identified. This suggest that currently, systems for genome mining and prediction of BGCs can efficiently identify AQ producing BGCs from known producers, but may fail to identify the same metabolic pathway in different groups of organisms, this might be due to a variety of reasons: structural differences in the machinery employed by different genera of microorganisms, which even though might possess the same core protein possess structurally different tailoring enzymes difference in the organization of the cluster itself, as in the order of genes or the presence and absence of additional genes as compared to known AQ BGCs structures from reference organisms and finally the activation of a production pathway for anthraquinones might be dependent on the activation of more than one BGC which might also requires a more complex regulatory system.

These are in accordance with current literature, and might be reasons for the abundance of "orphan" BGCs. Although currently, we were not able to link the presence of AQs molecule to the specific BGC producing it or to identify the conditions for its activation, future investigations might be devoted to studying and developing elicitation approaches and to confirming which BGC are required for the production of AQs through the use Knock-out strains, eventually linking the orphan BGC and its product. Eventually increasing knowledge on the structures of BGCs and allowing for a better recognition of

AQs producing BGCs from unreported strains but also as a necessary step for biotechnological implementation of AQs using heterologous hosts.

REFERENCES:

Abel, A. (2012). 24 - The history of dyes and pigments: From natural dyes to high performance pigments. Colour Design (Second Edition). J. Best, Woodhead Publishing**:** 557-587.

Alsukaibi, A. K. D. (2022). "Various Approaches for the Detoxification of Toxic Dyes in Wastewater." Processes **10**(10): 1968.

Altschul, S. F., W. Gish, W. Miller, E. W. Myers and D. J. Lipman (1990). "Basic local alignment search tool." J Mol Biol **215**(3): 403-410.

Baaka, N., I. El Ksibi and M. F. Mhenni (2017). "Optimisation of the recovery of carotenoids from tomato processing wastes: application on textile dyeing and assessment of its antioxidant activity." Natural Product Research **31**(2): 196-203.

Ballinger Jr, K. E. (2015). Use of quinone compound in building materials, Google Patents.

Barrera Vázquez, M. F., L. R. Comini, R. E. Martini, S. C. Núñez Montoya, S. Bottini and J. L. Cabrera (2014). "Comparisons between conventional, ultrasound-assisted and microwave-assisted methods for extraction of anthraquinones from Heterophyllaea pustulata Hook f. (Rubiaceae)." Ultrasonics Sonochemistry **21**(2): 478-484.

Blin, K., S. Shaw, M. H. Medema and T. Weber (2023). "The antiSMASH database version 4: additional genomes and BGCs, new sequence-based searches and more." Nucleic Acids Research.

Borchert, M. S., P. Nielsen, I. Graeber, I. Kaesler, U. Szewzyk, T. Pape, G. Antranikian and T. Schäfer (2007). "Bacillus plakortidis sp. nov. and Bacillus murimartini sp. nov., novel alkalitolerant members of rRNA group 6." International journal of systematic and evolutionary microbiology **57**(12): 2888-2893.

Carlos, C., L. B. Pereira and L. M. M. Ottoboni (2017). "Comparative genomics of Paracoccus sp. SM22M-07 isolated from coral mucus: insights into bacteria-host interactions." Current Genetics **63**(3): 509-518.

Chia, S. R., K. W. Chew, H. Y. Leong, S. Manickam, P. L. Show and T. H. P. Nguyen (2020). "Sonoprocessing-assisted solvent extraction for the recovery of pigment-protein complex from Spirulina platensis." Chemical Engineering Journal **398**: 125613.

Christner, B. C., B. H. Kvitko and J. N. Reeve (2003). "Molecular identification of Bacteria and Eukarya inhabiting an Antarctic cryoconite hole." Extremophiles **7**(3): 177-183.

Cova, T. F. G. G., A. A. C. C. Pais and J. S. Seixas De Melo (2017). "Reconstructing the historical synthesis of mauveine from Perkin and Caro: procedure and details." Scientific Reports **7**(1).
De Santis, D. and M. Moresi (2007). "Production of alizarin extracts from Rubia tinctorum and assessment of their dyeing properties." Industrial Crops and Products **26**(2): 151-162.
Deliberto, S. T. and S. J. Werner (2016). "Review of anthraquinone applications for pest management and agricultural crop protection." Pest Management Science **72**(10): 1813-1825.
Deng, Y., C.-J. Li, J. Zhang, W.-H. Liu, L.-Y. Yu and Y.-Q. Zhang (2024). "Extensive genomic study characterizing three

Paracoccaceae

populations and revealing

Pseudogemmobacter lacusdianii

sp. nov. and

Paracoccus broussonetiae

sp. nov." Microbiology Spectrum **12**(11).
Devi, N., R. Rajendran and S. K. Sundaram (2011). "Isolation and characterization of bioactive compounds from marine bacteria."
Di Marco, A., G. Cassinelli and F. Arcamone (1981). "The discovery of daunorubicin." Cancer Treat Rep **65**(Suppl 4): 3-8.
Diaz-Munoz, G., I. L. Miranda, S. K. Sartori, D. C. De Rezende and M. A. Diaz (2018). "Anthraquinones: an overview." Studies in natural products chemistry **58**: 313-338.
Distel, D. L., M. A. Altamia, Z. Lin, J. R. Shipway, A. Han, I. Forteza, R. Antemano, M. G. J. P. Limbaco, A. G. Tebo and R. Dechavez (2017). "Discovery of chemoautotrophic symbiosis in the giant shipworm Kuphus polythalamia (Bivalvia: Teredinidae) extends wooden-steps theory." Proceedings of the National Academy of Sciences **114**(18): E3652-E3658.
Duval, J., V. Pecher, M. Poujol and E. Lesellier (2016). "Research advances for the extraction, analysis and uses of anthraquinones: A review." Industrial Crops and Products **94**: 812-833.
Firn, R. D. and C. G. Jones (2000). "The evolution of secondary metabolism – a unifying model." Molecular Microbiology **37**(5): 989-994.
Fontmorin, J.-M., S. Guiheneuf, T. Godet-Bar, D. Floner and F. Geneste (2022). "How anthraquinones can enable aqueous organic redox flow batteries to meet the needs of industrialization." Current Opinion in Colloid & Interface Science **61**: 101624.
Fried, R., I. Oprea, K. Fleck and F. Rudroff (2022). "Biogenic colourants in the textile industry – a promising and sustainable alternative to synthetic dyes." Green Chemistry **24**(1): 13-35.
Gupta, R. S., S. Patel, N. Saini and S. Chen (2020). "Robust demarcation of 17 distinct Bacillus species clades, proposed as novel Bacillaceae genera, by phylogenomics and comparative genomic analyses: description of Robertmurraya kyonggiensis sp. nov. and proposal for an emended genus Bacillus limiting it only to the members of the Subtilis and Cereus clades of species." International Journal of Systematic and Evolutionary Microbiology **70**(11): 5753-5798.

Gurkok, S. (2022). "A novel carotenoid from Metabacillus idriensis LipT27: production, extraction, partial characterization, biological activities and use in textile dyeing." Archives of Microbiology **204**(6).
Hollensteiner, J., D. Schneider, A. Poehlein, T. Brinkhoff and R. Daniel (2023). "Pan-genome analysis of six Paracoccus type strain genomes reveal lifestyle traits." PLOS ONE **18**(12): e0287947.
Hou, Y., S. Cao, P. J. Brodie, M. W. Callmander, F. Ratovoson, E. A. Rakotobe, V. E. Rasamison, M. Ratsimbason, J. N. Alumasa, P. D. Roepe and D. G. I. Kingston (2009). "Antiproliferative and antimalarial anthraquinones of Scutia myrtina from the Madagascar forest." Bioorganic & Medicinal Chemistry **17**(7): 2871-2876.
Ivanova, E. P., Y. A. Alexeeva, N. V. Zhukova, N. M. Gorshkova, V. Buljan, D. V. Nicolau, V. V. Mikhailov and R. Christen (2004). "Bacillus algicola sp. nov., a novel filamentous organism isolated from brown alga Fucus evanescens." Systematic and applied microbiology **27**(3): 301-307.
Jaffer, Y. D., H. Sanath Kumar, R. Vinothkumar, A. B. Irfan, N. M. Ishfaq, P. A. Ganie, R. A. H. Bhat and A. Vennila (2019). "Isolation and characterization of heterotrophic nitrification–aerobic denitrification and sulphur-oxidizing bacterium Paracoccus saliphilus strain SPUM from coastal shrimp ponds." Aquaculture International **27**(5): 1513-1524.
Joshi, A., S. Thite, P. Karodi, N. Joseph and T. Lodha (2022). "Corrigendum: Alkalihalobacterium elongatum gen. nov. sp. nov.: An Antibiotic-Producing Bacterium Isolated From Lonar Lake and Reclassification of the Genus Alkalihalobacillus Into Seven Novel Genera." Frontiers in Microbiology **13**.
Kant, R. (2012). "Textile dyeing industry an environmental hazard." Natural Science **04**(01): 22-26.
Khankaew, S., A. Mills, D. Yusufu, N. Wells, S. Hodgen, W. Boonsupthip and P. Suppakul (2017). "Multifunctional anthraquinone-based sensors: UV, O2 and time." Sensors and Actuators B: Chemical **238**: 76-82.
Kim, S.-B., K. H. Kim and J.-S. Park (2024). "Paracoccus spongiarum sp. nov., isolated from the marine sponge, Phakellia elegans." International Journal of Systematic and Evolutionary Microbiology **74**(10).
Kumdhitiahutsawakul, L., D. Jirachaisakdeacha, U. Kantha, P. Pholchan, P. Sattayawat, T. Chitov, Y. Tragoolpua and S. Bovonsombut (2022). "Removal of Hydrogen Sulfide from Swine-Waste Biogas on a Pilot Scale Using Immobilized Paracoccus versutus CM1." Microorganisms **10**(11): 2148.
Kämpfer, P., R. Irgang, M. Poblete-Morales, G. Fernández-Negrete, S. P. Glaeser, D. Fuentes-Messina and R. Avendaño-Herrera (2019). "Paracoccus nototheniae sp. nov., isolated from a black rock cod fish (Notothenia coriiceps) from the Chilean Antarctic." International Journal of Systematic and Evolutionary Microbiology **69**(9): 2794-2800.
Lech, K. and M. Jarosz (2011). "Novel methodology for the extraction and identification of natural dyestuffs in historical textiles by HPLC–UV–Vis–ESI MS. Case study: chasubles from the Wawel Cathedral collection." Analytical and Bioanalytical Chemistry **399**(9): 3241-3251.
Leinberger, J., J. Holste, B. Bunk, H. M. Freese, C. Spröer, L. Dlugosch, A.-C. Kück, S. Schulz and T. Brinkhoff (2021). "High Potential for Secondary Metabolite Production of Paracoccus marcusii CP157, Isolated From the Crustacean Cancer pagurus." Frontiers in Microbiology **12**.
Lonkeng, L. T., P. Eckhardt, B. T. Tsafack, R. Forster, B. K. Ponou, R. B. Teponno, T. B. Nguelefack, T. Opatz and L. A. Tapondjou (2024). "Rhizomes of Rumex abyssinicus

Jacq.: Unveiling five new anthraquinones (Rumabynosides AE) and a review on hepatoprotective potential of its phytochemicals." Phytochemistry Letters **64**: 30-36.
Lu, C.-H., T.-H. Han, N. Jiang, X.-T. Gai, Z.-H. Cao, S.-Y. Zou, W. Chen, J.-H. Ma, Z.-L. Lin, J. Li, D.-Z. Liao, L.-Q. Zhang, Y. Jin and Z.-Y. Xia (2022). "Pseudomonas lijiangensis sp. nov., a novel phytopathogenic bacterium isolated from black spots of tobacco." International Journal of Systematic and Evolutionary Microbiology **72**(10).
Lyu, L., Q. Lai, J. Li, Z. Yu and Z. Shao (2021). "Paracoccus amoyensis sp. nov., isolated from the surface seawater along the coast of Xiamen Island, China." International Journal of Systematic and Evolutionary Microbiology **71**(3).
Malik, E. M. and C. E. Müller (2016). "Anthraquinones As Pharmacological Tools and Drugs." Medicinal Research Reviews **36**(4): 705-748.
Malmir, M., R. Serrano and O. Silva (2017). "Anthraquinones as potential antimicrobial agents-A review." Antimicrobial research: Novel bioknowledge and educational programs **20**: 55-61.
Margesin, R., P. Schumann, D.-C. Zhang, M. Redzic, Y.-G. Zhou, H.-C. Liu and F. Schinner (2012). "Arthrobacter cryoconiti sp. nov., a psychrophilic bacterium isolated from alpine glacier cryoconite." International Journal of Systematic and Evolutionary Microbiology **62**(2): 397-402.
Marković, Z., S. Jeremić, J. D. Marković, M. S. Pirković and D. Amić (2016). "Influence of structural characteristics of substituents on the antioxidant activity of some anthraquinone derivatives." Computational and Theoretical Chemistry **1077**: 25-31.
Masasa, M., A. Kushmaro, H. Chernova, N. Shashar and L. Guttman (2022). "Carbohydrate-Active Enzymes of a Novel Halotolerant

Alkalihalobacillus

Species for Hydrolysis of Starch and Other Algal Polysaccharides." Microbiology Spectrum **10**(4).
Mashabela, M. D., L. A. Piater, I. A. Dubery, F. Tugizimana and M. I. Mhlongo (2022). "Rhizosphere Tripartite Interactions and PGPR-Mediated Metabolic Reprogramming towards ISR and Plant Priming: A Metabolomics Review." Biology **11**(3): 346.
Mei, X., C. Wu, J. Zhao, T. Yan and P. Jiang (2019). "Community Structure of Bacteria Associated With Drifting Sargassum horneri, the Causative Species of Golden Tide in the Yellow Sea." Frontiers in Microbiology **10**.
Minotti, G., P. Menna, E. Salvatorelli, G. Cairo and L. Gianni (2004). "Anthracyclines: molecular advances and pharmacologic developments in antitumor activity and cardiotoxicity." Pharmacological reviews **56**(2): 185-229.
Modolon, F., A. R. Barno, H. D. M. Villela and R. S. Peixoto (2020). "Ecological and biotechnological importance of secondary metabolites produced by coral-associated bacteria." Journal of Applied Microbiology **129**(6): 1441-1457.
Moore, D., G. Robson and A. Trinci (2020). 21st Century Guidebook to Fungi.
Mortazavi, R., S. Attiya and P. Ariya (2014). "A next generation sequencing of Arctic bacteria in snow and frost flowers: identification, abundance and freezing nucleation." Atmospheric Chemistry & Physics Discussions **14**(23).
Mortazavi, R., C. T. Hayes and P. A. Ariya (2008). "Ice nucleation activity of bacteria isolated from snow compared with organic and inorganic substrates." Environmental Chemistry **5**(6): 373-381.
Narayanan, Z. and B. R. Glick (2022). "Secondary Metabolites Produced by Plant Growth-Promoting Bacterial Endophytes." Microorganisms **10**(10): 2008.

Neyrinck, A. M., J. Rodriguez, B. Taminiau, F. Herpin, P. D. Cani, G. Daube, L. B. Bindels and N. M. Delzenne (2022). "Constipation Mitigation by Rhubarb Extract in Middle-Aged Adults Is Linked to Gut Microbiome Modulation: A Double-Blind Randomized Placebo-Controlled Trial." International Journal of Molecular Sciences **23**(23): 14685.
Niinimäki, K., G. Peters, H. Dahlbo, P. Perry, T. Rissanen and A. Gwilt (2020). "The environmental price of fast fashion." Nature Reviews Earth & Environment **1**(4): 189-200.
Nitiss, J. L. (2009). "Targeting DNA topoisomerase II in cancer chemotherapy." Nature Reviews Cancer **9**(5): 338-350.
Palladino, G., E. Caroselli, T. Tavella, F. D'Amico, F. Prada, A. Mancuso, S. Franzellitti, S. Rampelli, M. Candela, S. Goffredo and E. Biagi (2022). "Metagenomic shifts in mucus, tissue and skeleton of the coral Balanophyllia europaea living along a natural CO2 gradient." ISME Communications **2**(1).
Patel, A., N. Arora, V. Pruthi and P. A. Pruthi (2019). "A novel rapid ultrasonication-microwave treatment for total lipid extraction from wet oleaginous yeast biomass for sustainable biodiesel production." Ultrasonics Sonochemistry **51**: 504-516.
Patel, O. P., R. M. Beteck and L. J. Legoabe (2021). "Antimalarial application of quinones: A recent update." European Journal of Medicinal Chemistry **210**: 113084.
Patra, A. K. and S. R. K. Pariti (2022). "Restricted substances for textiles." Textile Progress **54**(1): 1-101.
Paudel, P., H. A. Jung and J. S. Choi (2018). "Anthraquinone and naphthopyrone glycosides from Cassia obtusifolia seeds mediate hepatoprotection via Nrf2-mediated HO-1 activation and MAPK modulation." Archives of Pharmacal Research **41**(6): 677-689.
Posner, S. and C. Jönsson (2014). Chemicals in textiles-Risks to human health and the environment: Report from a government assignment, Swedish Chemicals Agency.
Prateeksha, P., R. Bajpai, C. V. Rao, D. K. Upreti, S. K. Barik and B. N. Singh (2021). "Chrysophanol-functionalized silver nanoparticles for anti-adhesive and anti-biofouling coatings to prevent urinary catheter-associated infections." ACS Applied Nano Materials **4**(2): 1512-1528.
Preet, G., J. Gomez-Banderas, R. Ebel and M. Jaspars (2022). "A structure-activity relationship analysis of anthraquinones with antifouling activity against marine biofilm-forming bacteria." Frontiers in Natural Products **1**.
Qiu, Q., Y. Gu, Y. Ren, H. Ding, C. Hu, D. Wu, J. Mou, Z. Wu and D. Dai (2024). "Research progress on eco-friendly natural antifouling agents and their antifouling mechanisms." Chemical Engineering Journal: 153638.
Quast, C., E. Pruesse, P. Yilmaz, J. Gerken, T. Schweer, P. Yarza, J. Peplies and F. O. Glöckner (2012). "The SILVA ribosomal RNA gene database project: improved data processing and web-based tools." Nucleic acids research **41**(D1): D590-D596.
Radovanović, N., M. Milutinović, K. Mihajlovski, J. Jović, B. Nastasijević, M. Rajilić-Stojanović and S. Dimitrijević-Branković (2018). "Biocontrol and plant stimulating potential of novel strain Bacillus sp. PPM3 isolated from marine sediment." Microbial Pathogenesis **120**: 71-78.
Raghuveer, D., V. V. Pai, T. S. Murali and R. Nayak (2023). "Exploring anthraquinones as antibacterial and antifungal agents." ChemistrySelect **8**(6): e202204537.
Rajasabapathy, R., S. C. Ghadi, B. Manikandan, C. Mohandass, A. Surendran, S. G. Dastager, R. M. Meena and R. A. James (2020). "Antimicrobial profiling of coral reef and sponge associated bacteria from southeast coast of India." Microbial Pathogenesis **141**: 103972.

Rausch, T., M. H.-Y. Fritz, A. Untergasser and V. Benes (2020). "Tracy: basecalling, alignment, assembly and deconvolution of sanger chromatogram trace files." BMC Genomics **21**(1).
Romanenko, L., N. Otstavnykh, N. Tanaka, V. Kurilenko, V. Svetashev, L. Tekutyeva, V. Mikhailov and M. Isaeva (2023). "Characterization and Genomic Analysis of Fererhizobium litorale gen. nov., sp. nov., Isolated from the Sandy Sediments of the Sea of Japan Seashore." Microorganisms **11**(10): 2385.
Sandy, M. and A. Butler (2009). "Microbial Iron Acquisition: Marine and Terrestrial Siderophores." Chemical Reviews **109**(10): 4580-4595.
Semple, S. J., S. M. Pyke, G. D. Reynolds and R. L. Flower (2001). "In vitro antiviral activity of the anthraquinone chrysophanic acid against poliovirus." Antiviral research **49**(3): 169-178.
Shen, N., J. Ren, Y. Liu, W. Sun, Y. Li, H. Xin and Y. Cui (2023). "Natural edible pigments: A comprehensive review of resource, chemical classification, biosynthesis pathway, separated methods and application." Food Chemistry **403**: 134422.
Shi, Y.-b., H.-l. Li, H.-q. Wang, Y.-b. Yang, X.-y. Zhang, H. Wang, Z.-j. Zhu, Z.-y. Zhang and C.-a. Zhang (2014). "Simultaneous determination of five anthraquinones in a Chinese traditional preparation by RP-HPLC using an improved extraction procedure." Journal of Integrative Medicine **12**(5): 455-462.
Singh, S., S. B. Nimse, D. E. Mathew, A. Dhimmar, H. Sahastrabudhe, A. Gajjar, V. A. Ghadge, P. Kumar and P. B. Shinde (2021). "Microbial melanin: Recent advances in biosynthesis, extraction, characterization, and applications." Biotechnology Advances **53**: 107773.
Song, H.-K., W. Song, M. Kim, B. M. Tripathi, H. Kim, P. Jablonski and J. M. Adams (2017). "Bacterial strategies along nutrient and time gradients, revealed by metagenomic analysis of laboratory microcosms." FEMS Microbiology Ecology **93**(10).
Song, L., H. Liu, J. Wang, Y. Huang, X. Dai, X. Han and Y. Zhou (2016). "Bacillus oceani sp. nov., isolated from seawater." International Journal of Systematic and Evolutionary Microbiology **66**(2): 796-800.
Sprouffske, K. and A. Wagner (2016). "Growthcurver: an R package for obtaining interpretable metrics from microbial growth curves." BMC Bioinformatics **17**(1).
Susilowati, P. E., D. Ardianti, S. Kartini, I. N. Sudiana and A. Zaeni (2021). "Isolation of Ureolytic Bacteria of Soft Coral and Their Potential in Microbially Induced Calcite Precipitation (MICP)." Journal of Physics: Conference Series **1899**(1): 012003.
Tkaczyk, A., K. Mitrowska and A. Posyniak (2020). "Synthetic organic dyes as contaminants of the aquatic environment and their implications for ecosystems: A review." Science of The Total Environment **717**: 137222.
Tyc, Olaf, C. Song, J. S. Dickschat, M. Vos and P. Garbeva (2017). "The Ecological Role of Volatile and Soluble Secondary Metabolites Produced by Soil Bacteria." Trends in Microbiology **25**(4): 280-292.
Varasteh, T., L. Hamerski, D. Tschoeke, A. S. Lima, G. Garcia, C. A. N. Cosenza, C. Thompson and F. Thompson (2021). "Conserved Pigment Profiles in Phylogenetically Diverse Symbiotic Bacteria Associated with the Corals Montastraea cavernosa and Mussismilia braziliensis." Microbial Ecology **81**(1): 267-277.
Velliky, E. C., M. Porr and N. J. Conard (2018). "Ochre and pigment use at Hohle Fels cave: Results of the first systematic review of ochre and ochre-related artefacts from the Upper Palaeolithic in Germany." PLOS ONE **13**(12): e0209874.
Vogel, H. J. (1956). "A convenient growth medium for Neurospora (Medium N)." Microbial Genet. Bull. **13**: 42-43.

Wada, A., M. Shoda, H. Kubota, T. Kobayashi, Y. Katayama-Fujimura and H. Kuraishi (1986). "Characteristics of H2S oxidizing bacteria inhabiting a peat biofilter." Journal of Fermentation Technology **64**(2): 161-167.
Wang, G., J. Liu, Y. Li, J. Li, J. Luo, B. Chen, Z. Liao, H. Su, J. Liang and K. Yu (2022). "Description of Prasinibacter corallicola gen. nov., sp. nov., a zeaxanthin-producing bacterium isolated from stony coral Porites lutea." Antonie van Leeuwenhoek **115**(7): 933-941.
Wick, R. R., L. M. Judd, C. L. Gorrie and K. E. Holt (2017). "Unicycler: Resolving bacterial genome assemblies from short and long sequencing reads." PLOS Computational Biology **13**(6): e1005595.
Williams, D. H. and R. A. Maplestone Why are Secondary Metabolites Biosynthesized? Sophistication in the Inhibition of Cell Wall Biosynthesis by Vancomycin Group Antibiotics. Ciba Foundation Symposium 171 - Secondary Metabolites: their Function and Evolution**:** 45-63.
Williams, D. H., M. J. Stone, P. R. Hauck and S. K. Rahman (1989). "Why Are Secondary Metabolites (Natural Products) Biosynthesized?" Journal of Natural Products **52**(6): 1189-1208.
Wu, C. C., Y. C. Li, Y. R. Wang, T. K. Li and N. L. Chan (2013). "On the structural basis and design guidelines for type II topoisomerase-targeting anticancer drugs." Nucleic Acids Res **41**(22): 10630-10640.
Xiang, W., Q.-S. Song, H.-J. Zhang and S.-P. Guo (2008). "Antimicrobial anthraquinones from Morinda angustifolia." Fitoterapia **79**(7-8): 501-504.
Yang, L., Y. Wan, W. Li, C. Liu, H.-F. Li, Z. Dong, K. Zhu, S. Jiang, E. Shang, D. Qian and J. Duan (2022). "Targeting intestinal flora and its metabolism to explore the laxative effects of rhubarb." Applied Microbiology and Biotechnology **106**(4): 1615-1631.
Yashiro, E., R. N. Spear and P. S. Mcmanus (2011). "Culture-dependent and culture-independent assessment of bacteria in the apple phyllosphere." Journal of Applied Microbiology **110**(5): 1284-1296.
Yildirim, K., A. Akalin-Baskaya and M. L. Hidayetoglu (2007). "Effects of indoor color on mood and cognitive performance." Building and Environment **42**(9): 3233-3240.
Yoon, J.-H., I.-G. Kim, K. H. Kang, T.-K. Oh and Y.-H. Park (2004). "Bacillus hwajinpoensis sp. nov. and an unnamed Bacillus genomospecies, novel members of Bacillus rRNA group 6 isolated from sea water of the East Sea and the Yellow Sea in Korea." International Journal of Systematic and Evolutionary Microbiology **54**(3): 803-808.
Zari, S. T. and T. A. Zari (2015). "A review of four common medicinal plants used to treat eczema." Journal of Medicinal Plants Research **9**(24): 702-711.
Zhang, F., Q. Ye, Q. Chen, K. Yang, D. Zhang, Z. Chen, S. Lu, X. Shao, Y. Fan, L. Yao, L. Ke, T. Zheng and H. Xu (2018). "Algicidal Activity of Novel Marine Bacterium Paracoccus sp. Strain Y42 against a Harmful Algal-Bloom-Causing Dinoflagellate, Prorocentrum donghaiense." Applied and Environmental Microbiology **84**(19).
Zhang, K., Q. Zeng, R. Jiang, S. Shi, J. Yang, L. Long and X. Tian (2023). "Three Novel Marine Species of Paracoccus, P. aerodenitrificans sp. nov., P. sediminicola sp. nov. and P. albus sp. nov., and the Characterization of Their Capability to Perform Heterotrophic Nitrification and Aerobic Denitrification." Microorganisms **11**(6): 1532.
Zhou, Y. and R.-C. Tang (2016). "Modification of curcumin with a reactive UV absorber and its dyeing and functional properties for silk." Dyes and Pigments **134**: 203-211.

Chrismas, N. and M. Cunliffe (2020). "Depth-dependent mycoplankton glycoside hydrolase gene activity in the open ocean—evidence from the Tara Oceans eukaryote metatranscriptomes." The ISME Journal **14**(9): 2361-2365.
Cunliffe, M., A. Hollingsworth, C. Bain, V. Sharma and J. D. Taylor (2017). "Algal polysaccharide utilisation by saprotrophic planktonic marine fungi." Fungal Ecology **30**: 135-138.
Muriel, J. N., J. M. Bruque, J. M. Ol�As and A. Jim�Nez-S�Nchez (1996). "Production of biosurfactants by Cladosporium resinae." Biotechnology Letters **18**(3).
Olm, M. R., C. T. Brown, B. Brooks and J. F. Banfield (2017). "dRep: a tool for fast and accurate genomic comparisons that enables improved genome recovery from metagenomes through de-replication." The ISME Journal **11**(12): 2864-2868.
Parks, D. H., M. Imelfort, C. T. Skennerton, P. Hugenholtz and G. W. Tyson (2015). "CheckM: assessing the quality of microbial genomes recovered from isolates, single cells, and metagenomes." Genome Research **25**(7): 1043-1055.
Salvatore, M. M., A. Andolfi and R. Nicoletti (2021). "The Genus Cladosporium: A Rich Source of Diverse and Bioactive Natural Compounds." Molecules **26**(13): 3959.
Singh, S., S. B. Nimse, D. E. Mathew, A. Dhimmar, H. Sahastrabudhe, A. Gajjar, V. A. Ghadge, P. Kumar and P. B. Shinde (2021). "Microbial melanin: Recent advances in biosynthesis, extraction, characterization, and applications." Biotechnology Advances **53**: 107773.
Skinnider, M. A., C. W. Johnston, M. Gunabalasingam, N. J. Merwin, A. M. Kieliszek, R. J. Maclellan, H. Li, M. R. M. Ranieri, A. L. H. Webster, M. P. T. Cao, A. Pfeifle, N. Spencer, Q. H. To, D. P. Wallace, C. A. Dejong and N. A. Magarvey (2020). "Comprehensive prediction of secondary metabolite structure and biological activity from microbial genome sequences." Nature Communications **11**(1).
Tran-Ly, A. N., C. Reyes, F. W. M. R. Schwarze and J. Ribera (2020). "Microbial production of melanin and its various applications." World Journal of Microbiology and Biotechnology **36**(11).

RINGRAZIAMENTI:

Desidero ringraziare per il supporto ricevuto, in questi ormai terminate tre anni di lavoro, in primis il mio relatore Prof. Marco Candela per la pazienza ed esperienza che ha dimostrato nel guidarmi in tutte le scelte necessarie per fare progredire questa ricercar e senza il quale non avrei potuto terminare questo lavoro.

Vorrei inoltre ringraziare tutti colleghi con quali ho passato ore in laboratorio e che hanno potuto aiutarmi o insegnarmi in questi tre anni facendomi crescere sia professionalmente che umanamente.